2010

Closed Time-like Curves and Inertial Frame Dragging: How to Time Travel via Spacetime Rotation

Conrad Wilson Moore
Bucknell University

CLOSED TIME-LIKE CURVES AND INERTIAL FRAME DRAGGING: HOW TO TIME TRAVEL VIA SPACETIME ROTATION

by

Conrad Moore

A Thesis

Presented to the Faculty of

Bucknell University

in Partial Fulfillment of the Requirements for the Degree of

Bachelor of Science with Honors in Physics & Astronomy

May 3, 2010

Approved:

Dr. Jeffrey Bowen
Thesis Advisor

Dr. David Schoepf
Chair, Department of Physics & Astronomy

Contents

List of Tables

List of Figures

Abstract

As the number of solutions to the Einstein equations with realistic matter sources that admit closed time-like curves (CTC's) has grown drastically, it has provoked some authors [10] to call for a physical interpretation of these seemingly exotic curves that could possibly allow for causality violations. A first step in drafting a physical interpretation would be to understand how CTC's are created because the recent work of [16] has suggested that, to follow a CTC, observers must counter-rotate with the rotating matter, contrary to the currently accepted explanation that it is due to inertial frame dragging that CTC's are created. The exact link between inertial frame dragging and CTC's is investigated by simulating particle geodesics and the precession of gyroscopes along CTC's and backward in time oriented circular orbits in the van Stockum metric, known to have CTC's that could be traversal, so the van Stockum cylinder could be exploited as a time machine. This study of gyroscope precession, in the van Stockum metric, supports the theory that CTC's are produced by inertial frame dragging due to rotating spacetime metrics.

Chapter 1

Introduction

The possibility of traveling back in time has always captured the imagination and is a common plot device in science fiction. While such possibilities appear fanciful, Einstein's equations and the mathematics of general relativity do allow warping of spacetime that result in paths that a timelike observer (an observer that has mass and never locally exceeds the speed of light) could follow and visit certain events in the past.

1.1 Motivation in Brief

There are now a number of solutions to the Einstein equations with realistic matter sources that exhibit this possibly causality violating behavior [10] via the creation of what are called closed timelike curves (CTC's). The question becomes are CTC's just pathological mathematics or are they real physical phenomenon and therefore require the development of a physical interpretation as to their implications? Several authors, in particular [10] and [15], have taken this latter position and have argued that a more satisfying physical interpretation is needed. Aside from their properties, a current unsettled question is what is it that creates CTC's in the first place. The status quo is that inertial frame dragging, a phenomenon caused by rotating spacetimes, is what creates CTC's [16] [4]. However, the recent work of [16] has challenged this established view. As inertial frame dragging is a source of gyroscope precession, its relationship with the generation of CTC's could, conceivably, be quantified by simulating how

spin orientations precess along CTC's or in regions of backward time travel.

1.2 The Story of Closed Time-like Curves

Curious temporal behavior associated with CTC's has been objected to on the grounds that such behavior is due to periodicity imposed in particular coordinates [8] [4], or due to exotic or simply injudicious choices of topology [2] [4] (wormhole geometries would fall into this category). In short, causality violating behavior is discounted on the belief that it is due to pathological mathematics and unphysical geometries (geometries that no realistic matter sources could create) rather than any real physics of general relativity, as mentioned in Sec 1.1.

Despite these objections, there is a growing number of solutions to the Einstein equations with realistic matter sources that create regions in spacetime that allow for the possibility of causality violations, for example, a particle being able to meet itself at the same spatial coordinates with no coordinate time having elapsed, or being able to visit any point in its past (more discussion on the interpretation of CTC's will be presented in Chap 2.7). The Kerr solution for a rotating, spherically symmetric mass (a rotating black hole or star) was found to exhibit CTC's by Carter in [9]. However, the ability for terrestrial observers to ever witness such exotic behavior is objected because the CTC's loop through the interior and so the actual body, say the star, is expected to block observers from accessing them [9], and furthermore, this region is inside an event horizon and so observers outside the horizon would never be able to observe them [2]. The Kerr solution is expected to be the unique final state of gravitational collapse [2], and so the metric is entirely physical. The fact that CTC's exist in the solution makes it plausible that realistic matter sources could generate traversible CTC's, but, for the reasons just listed, it is unlikely that a Kerr black hole can be exploited and used as a time machine.

Another physical metric that exhibits CTC's is the van Stockum metric which is the solution of an infinitely long rotating cylinder of dust [3]. What makes the van Stockum solution important in the study of CTC's is that it is a physical solution, having non-exotic matter and topology. In this metric, CTC's emerge in the exterior vacuum region (discovered by Tipler in [2], incredibly many years after van Stockum's original discovery) not hidden behind horizons, implying that an observer could use it as a time machine if they were the correct distance away, in a causality violating region. The van Stockum metric is not without objection, namely that the geometry

is not asymptotically Minkowskian, as will be further discussed in Chap 4.2, and that it is of infinite mass. However, Tipler, in [2], argues that the infinite cylinder in Newtonian gravitation also does not vanish at infinity and, yet, it is a perfectly fine approximation for near a long finite cylinder.

More recently, Bonnor has observed how the library of solutions with CTC's and realistic "mundane" matter sources has been steadily growing, himself showing that the geometry of a mass-less rotating rod exhibits CTC's and arguing that the addition of mass would not eliminate them. It is Bonnor, in particular, who has called for a realistic physical interpretation of CTC's [10]. See [10] also for a collection of the literature for solutions with CTC's.

1.3 Overview

Bonnor's appeal for a physical interpretation is, in part, what motivates this numerical study of CTC's, although we do not attempt to provide an overarching physical interpretation for CTC's. What this paper is motivated by is the claim of Slobodov and others that "CTC's are produced by the *frame dragging* effect of the rotating matter" [4], while Andréka et. al., in [16], have claimed this is not the entire story. So what is needed is the development of methods to better understand this link between inertial frame dragging and the more exotic behavior of CTC's, and what role frame dragging actually plays in their creation. As Carter comments [9], the acceptability of Einstein's theory hinges on its predictions and so exploring the physical nature of CTC's could potentially point to needed revisions or inconsistencies in the theory.

Chap 2 is a basic introduction to the theory of relativity that, broadly, includes discussion of the needed notation, conventions and geometric ideas. In addition, the idea of causality is discussed, the basic equations of motion are introduced and the phenomenon of inertial frame dragging, CTC's and their hypothesized link is discussed. Chap 3 considers the precession of gyroscopes in more depth, specifically for the Schwarzschild geometry. The spacetime geometries specific to this paper are presented in Chap 4 and the numerical methods are discussed in Chap 5. Finally, results are presented in Chap 6.

Chapter 2

Overview of the Theory of General Relativity

In short, Einstein's theory of general relativity is a geometrical theory that describes gravity as the result of curvature in four dimensional spacetime. This curvature is mathematically described by the metric tensor which is directly related, via the Einstein equations, to the stress-energy (mass, momentum density, pressures and shears) of a source.

Flat space is a solution to the Einstein equations when there are no matter sources, but the addition of matter gives more nontrivial geometries which create relative accelerations between geodesics which is said to be the result of *gravity*. So, matter is what curves spacetime: it is what endows spacetime with geometry that deviates from flat space, hence *curving* it. Just as the geometry of an apple constrains how ants can move about on its surface, the local geometry, flat or curved, of spacetime and the mathematics of differential geometry constrain the way in which particles and observers can move [12]. The most important type of motion (because of its simplicity) is *geodesic* motion: motion where the observer is freely falling, under the influence of no forces, so the instructions for particle motion are entirely due to the curvature of spacetime. Therefore, calculating geodesics is a primary technique to explore the behavior of a particular geometry.

In this chapter, I introduce the necessary mathematics of tensors needed to understand spacetime geometry. For more full discussion see [1], [11], [12].

2.1 Coordinates, Vectors, Conventions and Notation

In a particular coordinate system, any point in space can be located by a set of numbers, each called a *coordinate*. For example, in Cartesian coordinates, in four dimensional spacetime, any point can be specified by the coordinates t, x, y, z. A common and powerful notation to write this in is:

$$x^\mu = \begin{pmatrix} t \\ x \\ y \\ z \end{pmatrix} , \tag{2.1}$$

where $\mu \in \{0, 1, 2, 3\}$, so Eq 2.1 is a convenient way to write $x^0 = t,\ x^1 = x,\ x^2 = y$ and $x^3 = z$. The *four vector* $\mathbf{x}$ [1] has components x^μ, and so is called a contravariant vector because the μ is in the upper position. There is no difference between contravariant vectors and the vectors encountered in normal introductory physics, but the notation will prove both convenient and powerful.

Given a coordinate system, such as Eq 2.1, a vector can be written in terms of a *coordinate basis* where the coordinate basis vectors are:

$$\mathbf{e}_\mu = \frac{\partial}{\partial x^\mu} = \partial_\mu, \tag{2.2}$$

or the directional derivative along the particular coordinate basis component. For example, $\mathbf{e}_0 = \ (1, 0, 0, 0)$, and so on. It should be noted that here μ does not denote a μ'th component, but the μ'th basis vector.

An important convention in general relativity is the Einstein summation convention in which repeated upper and lower indices are summed over the range of the indices:

$$x^\mu x_\mu = x^0 x_0 + x^1 x_1 + x^2 x_2 + x^3 x_3. \tag{2.3}$$

Following this convention, the four vector $\mathbf{x}$ can be conveniently written in terms of its coordinate basis as

$$\boldsymbol{x} = x^\mu \boldsymbol{e}_\mu. \tag{2.4}$$

[1] boldface will always denote four vectors and the usual spatial vectors will be denoted $\vec{x}$

2.2 The Metric Tensor and Spacetime Geometry

The metric tensor is a mathematical object that describes the curvature of a spacetime. Intuitively, it extends the idea of distance in 3 dimensional Euclidean geometry to abstract multi-dimensional space, and generalizes many familiar ideas.

2.2.1 The metric tensor and covariant tensors

The metric is a second rank, having $4^2 = 16$ components, symmetric tensor, an object that preserves the linear relations between two vectors in any basis. It can be represented as a 4×4 matrix. The metric summarizes the geometry and curvature of spacetime and is represented as $g_{\mu\nu}$ where the two indices range from 0 to 3, unless otherwise specified.

x_μ is called a covariant vector (the index is in the *co* or *low* position) and is related to its corresponding contravariant form via the metric, as

$$x_\mu = g_{\mu\nu} x^\nu \quad , \tag{2.5}$$

where the summation convention is implied. This is also called lowering an index, raising an index follows a similar construction. Note here the metric is written in its covariant form. The contravariant and covariant forms of the metric are related as

$$g_{\mu\alpha} g^{\alpha\nu} = g^\nu_\mu = \delta^\nu_\mu, \tag{2.6}$$

following the raising and lowering index rules, where δ is the Kronecker delta, and so the two forms are inverses.

With the metric $\mathbf{g}$, the dot product between the two four vectors $\mathbf{v}$ and $\mathbf{w}$ is

$$\mathbf{v} \cdot \mathbf{w} = g_{\mu\nu} v^\mu w^\nu, \tag{2.7}$$

and the angle θ between them is defined as

$$\cos\theta = \frac{v_a w^a}{|v_b v^b|^{1/2} |w_c w^c|^{1/2}}. \tag{2.8}$$

2.2.2 The geometry of flat space

The metric tensor summarizes all the information about the curvature of a space, as can be seen in flat space. The *line element* of a space describes the geometry of that space: it specifies how distance is measured. In 3-dimensional Euclidean space, the line element is just the Pythagorean theorem

$$ds^2 = dx^2 + dy^2 + dz^2. \tag{2.9}$$

However, when the dimension of time is added, becoming 4 dimensional Minkowski spacetime, the line element takes the form

$$ds^2 = -dt^2 + dx^2 + dy^2 + dz^2, \tag{2.10}$$

where Eq 2.10 has been written in geometrized units in which the speed of light c is set equal to unity. Throughout this paper,unless otherwise stated, units are chosen such that the speed of light c and the gravitational constant G are both set equal to unity. The general form for a line element takes the form

$$ds^2 = g_{\mu\nu} dx^\mu dx^\nu, \tag{2.11}$$

where the Einstein summation convention is assumed and $g_{\mu\nu}$ is the metric tensor. The components of the metric tensor for Eq 2.10 is, therefore,

$$g_{\mu\nu} = \eta_{\mu\nu} = \begin{pmatrix} -1 & 0 & 0 & 0 \\ 0 & 1 & 0 & 0 \\ 0 & 0 & 1 & 0 \\ 0 & 0 & 0 & 1 \end{pmatrix} . \tag{2.12}$$

where η is adopted to specifically refer to flat space. The metric tensor is connected to geometry because it is obtained directly from the line element, as shown. To further motivate this geometric interpretation, if the three dimensional identity matrix is used in Eq 2.11, then the Pythagorean theorem is recovered.

Coordinate and orthonormal basis

From the definition of the coordinate basis vectors in Eq 2.2 we can write the infinitesimal displacement vector in a coordinate basis as,

$$d\mathbf{s} = dx^\mu \mathbf{e}_\mu \tag{2.13}$$

which implies

$$ds^2 = d\mathbf{s} \cdot d\mathbf{s} = \mathbf{e}_\mu \cdot \mathbf{e}_\nu dx^\mu dx^\nu, \tag{2.14}$$

and, from comparison with Eq 2.11, conclude that [14]

$$\mathbf{e}_\mu \cdot \mathbf{e}_\nu = g_{\mu\nu} \tag{2.15}$$

which, therefore, is true for a coordinate basis. The definition of an orthonormal basis $\mathbf{e}_{\hat{\mu}}$ is

$$\mathbf{e}_{\hat{\mu}} \cdot \mathbf{e}_{\hat{\nu}} = \eta_{\hat{\mu}\hat{\nu}}. \tag{2.16}$$

However, the two bases are similar when their components are written explicitly. The coordinate components of the coordinate basis are, as mentioned before,

$$(\mathbf{e}_\mu)^\nu = \delta^\nu_\mu, \tag{2.17}$$

and the orthonormal components of the orthonormal basis are

$$(\mathbf{e}_{\hat{\mu}})^{\hat{\nu}} = \delta^{\hat{\nu}}_{\hat{\mu}}. \tag{2.18}$$

The bases can be "mixed" to calculate, for example, the orthonormal components of the coordinate basis[1]

$$(\mathbf{e}_\mu)^{\hat{\nu}} \tag{2.19}$$

and so on.

What is important about an orthonormal basis and the other mixed bases is that they allow for a way to perform calculations with respect to a local inertial frame (the choice of which basis is guided by convenience) which corresponds to the actual physical quantity that would be measured by a local observer. An explicit use of this is in Sec. 2.5 to reveal a rather bizarre phenomenon associated with the geometries of rotating bodies.

2.2.3 Light cones: the notion of causality

As Minkowski geometry is pseudo-Euclidean, straight (in the Euclidean sense) lines can be drawn to represent distances (although the magnitudes are *not* represented by the length of the lines because the geometry is not Euclidean) and so Eq 2.10 can be written as displacements in Cartesian coordinates:

$$(\Delta s)^2 = -(\Delta t)^2 + (\Delta x)^2 + (\Delta y)^2 + (\Delta z)^2. \tag{2.20}$$

Time is a fundamentally different *kind* of coordinate than space, represented by the negative on the g_{00} component of the metric tensor. It is important to differentiate between timelike types of distances (squared lengths that are negative) and spacelike types of distances (squared lengths that are positive). An inspection of Eq 2.20 suggests the distinctions can be written as three cases[1]:

Spacelike separated $(\Delta s)^2 > 0$.

Null separated $(\Delta s)^2 = 0$.

Timelike separated $(\Delta s)^2 < 0$.

The null separated distances are the lines that light rays travel along. Starting at an event P and drawing all outgoing null rays and all incoming possible light rays, forms a cone in Cartesian coordinates, as shown in Fig 2.1. These light cones are what determine our notion of causality: causal events must be timelike separated and for an event to cause another, say P causes A, then A must be in the future light cone of P. However, as mentioned, spacetime can be curved in such a way that a particle could travel into its past, and yet have its four velocity remain timelike, always pointing in the direction of the forward lightcone which would satisfy the conditions of the discussion in this section. This is where violations of causality could become a problem and where CTC's complicate our notion of causality. More discussion of CTC's and light cones is in Sec 2.7.

2.3 Equations of Motion in Curved Spacetime

In order to plot both particle trajectories and calculate the orientations of gyroscopes in curved spacetime, we will need the basic equations of motion for timelike freely-falling particles. The importance of the freely falling condition is that the equations are then entirely dependent on the metric tensor and the geometry of spacetime, taking their simplest form.

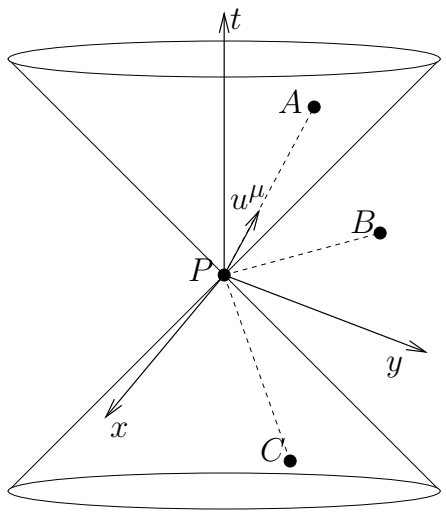

Figure 2.1: Light cone in flat space drawn at event P. A lies within the the forward light cone of P and so $(\Delta s_{PA})^2 < 0$ and P can be a *cause* of event A. Likewise, $(\Delta s_{PC})^2 < 0$ and C lies in the past of P and so can be a cause of P. $(\Delta s_{PB})^2 > 0$ and so P and B are spacelike separated. The orderings of spacelike separated events can be changed by a Lorentz transformation, or moving to a different frame. In the frame of the figure, P comes before B, but in a different frame B could very well come before P. This does not violate causality because if they are spacelike separated they cannot be causal. There is no Lorentz transformation that reverses the ordering of C, P and A. This appeals to our notion of causality: if an event causes another, it should be true in all frames.

2.3.1 The geodesic equation

One of the most effective general ways to probe the behavior of an abstract spacetime is to study the motion of *test particles*, particles that have such small mass that they do not perceptibly affect the spacetime curvature around them with their own mass. We now consider the equation of motion for such a particle. All timelike particles have their own internal 'clock' and *proper time*. An infinitesimal duration of proper time, $d\tau$, is defined as

$$-d\tau^2 = ds^2 = g_{\mu\nu} dx^\mu dx^\nu. \tag{2.21}$$

This definition is motivated by the distinction between spatial and temporal components: if the right hand side of Eq 2.21 is negative then the squared distance ds^2 is negative and, to avoid any discussion of complex numbers, negative squared distances are called timelike and are parametrized by τ instead. Proper time is an invariant

because it is related to ds^2 which is independent of coordinate systems. Therefore, it is a suitable parameter to parametrize a timelike path in spacetime as any observer can read a particle's own "watch". A particle's 4-velocity can now be defined as

$$u^\mu = \frac{dx^\mu}{d\tau}, \tag{2.22}$$

or the tangent to the world line, $x^\mu(\tau)$, parametrized by proper time τ.

The Lagrangian generalized to curved spacetime is written [11]

$$\mathcal{L} = g_{\mu\nu}\dot{x}^\mu\dot{x}^\nu, \tag{2.23}$$

where a dot represents a derivative with respect to an arbitrary parameter and for clarity it is assumed we are always talking about timelike world lines and so, unless otherwise stated, a dot is a derivative with respect to proper time, τ. The geodesic equation, the equation of motion we seek, is derived from this "Lagrangian" and the techniques of Lagrangian mechanics. Recalling the Euler-Lagrange equations

$$\frac{d}{d\tau}\left(\frac{\partial\mathcal{L}}{\partial\dot{x}^\mu}\right) - \frac{\partial\mathcal{L}}{\partial x^\mu} = 0, \tag{2.24}$$

we insert Eq 2.23, which yields the equation of motion, the geodesic equation:

$$\frac{d^2x^\mu}{d\tau^2} = -\Gamma^\mu_{\alpha\beta}\frac{dx^\alpha}{d\tau}\frac{dx^\beta}{d\tau}, \tag{2.25}$$

where $\Gamma^\mu_{\alpha\beta}$ are called the connection coefficients. They can be expressed as derivatives of the metric, or

$$\Gamma^\alpha_{\beta\gamma} = \frac{1}{2}g^{\alpha\delta}\left(\frac{\partial g_{\delta\beta}}{\partial x^\gamma} + \frac{\partial g_{\delta\gamma}}{\partial x^\beta} - \frac{\partial g_{\beta\gamma}}{\partial x^\delta}\right). \tag{2.26}$$

If all the Γ's are zero, as they would be in flat space in Cartesian coordinates 2.10, Eq 2.25 is simply the law of inertia [1], so it is certainly the equation of motion expected. Eq 2.25 is a system of four coupled second order differential equations that governs how the coordinate position of a test particle will change with proper time ($x^\mu(\tau)$). This geodesic equation can then be used to plot the particle trajectories; it is this equation that will be integrated to plot numerical simulations of test particle trajectories.

Dividing through by proper time in Eq 2.21, shows that, for timelike particles (particles parametrized by proper time), the four velocities must obey the following normalization:

$$\boldsymbol{u}\cdot\boldsymbol{u} = g_{\mu\nu}u^\mu u^\nu = -1. \tag{2.27}$$

This also justifies the definition of the Lagrangian Eq 2.23 because it is a constant term related to the positions, from the metric, and the squares of velocities which is loosely analogous to potential and kinetic energies. However, for light rays proper time does not advance ($d\tau = 0$) and so light rays (null lines) are parametrized by an affine parameter λ such that the similar equation

$$\boldsymbol{u} \cdot \boldsymbol{u} = g_{\mu\nu} \frac{dx^\mu}{d\lambda} \frac{dx^\nu}{d\lambda} = 0, \tag{2.28}$$

is true. Null lines are not calculated in this paper, but it is essential to see that, although parametrized and normalized differently, null lines follow Eq 2.25 and so they too are deflected by spacetime curvature. Therefore, light cones, which form the causal structure of a spacetime, can be distorted by non-flat geometries. It is this distortion, in particular ways, which can lead to regions of causality violation as discussed in Chap 2.7.

2.3.2 The Gyroscope Equation

A goal of this paper is to quantify the inertial frame dragging of a spacetime exhibiting CTC's. Inertial frame dragging causes gyroscopes to precess and also makes particles with initial zero angular momentum acquire some. In order to perform numerical simulations of the effect of inertial frame dragging, the mathematics governing the motion of spins in curved spacetime is discussed here.

As the geodesic equation determines the equation of motion for *test particles*, the gyroscope equation governs the orientation of spins for *test gyros*. The spin of a gyroscope is described by the four vector s^α. The spin four vector must be a spatial vector in the local inertial frame of an observer, meaning $s^\alpha = (0, \vec{s})$, and so $\boldsymbol{s} \cdot \boldsymbol{u} = 0$ at all points along a particle's world line because $\boldsymbol{u}$ is always timelike. Accordingly, because it is a spatial four vector, the magnitude of the spin, $\sqrt{\boldsymbol{s} \cdot \boldsymbol{s}}$, is a positive constant, denoted s_*, taken to be 1 in this paper. It is no surprise, as the spin of a gyroscope must be parallel transported[2] along with the four velocity [11], that the gyroscope equation takes the similar form:

$$\frac{ds^\alpha}{d\tau} + \Gamma^\alpha_{\beta\gamma} s^\beta u^\gamma = 0, \tag{2.29}$$

[2]In Eq 2.25, the four velocity vectors are said to be parallel transported along the particle's world line by the connection coefficients.

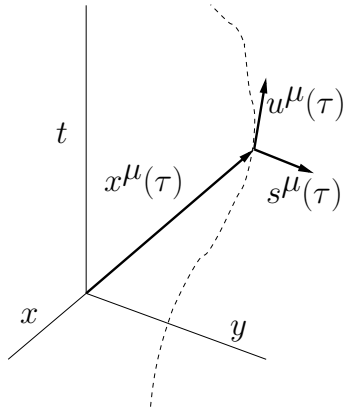

Figure 2.2: A summary of the coordinates and vectors. u^μ is tangent to the world line parametrized by τ and is plotted in the coordinates x^μ. Note that u^μ is drawn perpendicular to s^μ to reflect the condition $\mathbf{s} \cdot \mathbf{u} = 0$.

where $u^\alpha(\tau)$ is the timelike four velocity of the gyroscope. This equation can also be derived, more directly, from the definition of the spin four vector: because $\boldsymbol{s} \cdot \boldsymbol{u} = 0$, then

$$\frac{d}{d\tau}(\boldsymbol{s} \cdot \boldsymbol{u}) = 0, \tag{2.30}$$

and by using the geodesic equation and working out the necessary derivatives, the gyroscope equation can be derived. The spin of the gyroscope remains fixed in a local inertial frame where the metric becomes Eq 2.10, and this can be seen because all the Γ's would vanish because all the derivatives are trivial, as flat space has no coordinate dependence.

The list of four vectors involved has grown, and so a summary of the various vectors is provided in Fig 2.2, for convenience.

2.4 Geodetic Precession

An explicit example of geodetic precession will be provided in Chap 3.1.2 for the Schwarzschild geometry, but the idea will be presented here. Geodetic precession is the precession of a gyroscope that a particle carries with it, as it orbits about a massive body, with respect to a gyroscope orientated in a locally flat coordinate system of an instantaneously co-moving observer. From Eq 2.29, the spin of the gyroscope that

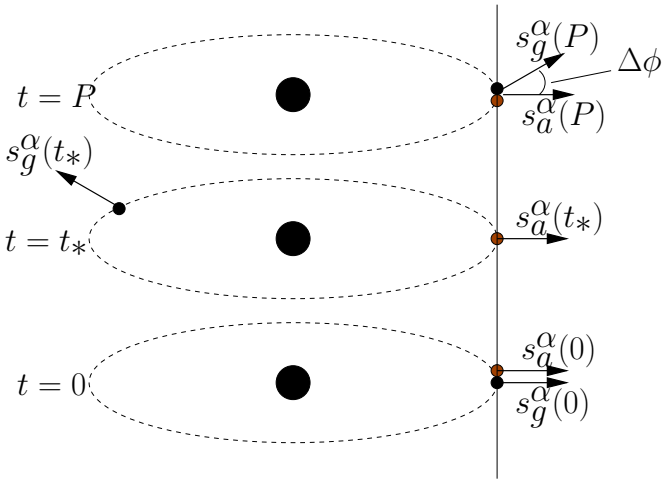

Figure 2.3: Consider a gyroscope, denoted observer g, in orbit about a black hole, in the Schwarzschild geometry. Another observer, denoted a, remains stationary in a local inertial frame. At $t = 0$, the observers have their gyroscopes orientated in the same radial direction , along a radial line drawn from the singularity in the equatorial plane. As a does not travel along a geodesic because straight lines are not geodesics in the Schwarzschild geometry, its spin vector is not Fermi-Walker transported while observer g's spin vector is. After observer g returns in a time of one orbital period $(2\pi/\Omega)$, observer g and a will both measure a precession angle $\Delta\phi$ due to this difference in transport. An arbitrary time t_* is also shown.

the orbiting particle carries with it is Fermi-Walker transported[3] while the co-moving particle's spin is not. This phenomenon is further described in Fig 2.3.

2.5 Inertial Frame Dragging

General relativity predicts that the inertial frames of special relativity are "dragged" in the vicinity of a rotating body [1] and this causes an additional precessional effect. The general stationary axisymmetric metric of a massive body rotating about its axis

[3]As gyroscopes can define the orthonormal tetrad of basis vectors that a particle carries with it, the only "rotation" is a result of the variance of the basis as it is transported through curved space. This is the definition of Fermi-Walker transport.

of symmetry takes the form [13]:

$$ds^2 = -e^{2\nu}dt^2 + e^{2\psi}(d\phi - \omega dt)^2 + e^{2\mu_2}(dx^2)^2 + e^{2\mu_3}(dx^3)^2, \tag{2.31}$$

where t and ϕ are the temporal and azimuthal angle about the axis of symmetry, respectively; x^2 and x^3 are the remaining spacial coordinates (they will turn out to be r and z in the van Stockum rotating cylinder case) and ω, ν, ψ, μ_2, and μ_3 are functions of x^2 and x^3 only (a result of the assumptions of axial symmetry and the stationary nature).

To demonstrate the dragging of inertial frames we first consider an arbitrary point in spacetime where a particle has the four velocity

$$u^\mu = \begin{pmatrix} u^t \\ u^t\Omega \\ u^t v_2 \\ u^t v_3 \end{pmatrix}, \tag{2.32}$$

where $u^1 = d\phi/d\tau = u^t d\phi/dt = u^t\Omega$ from the chain rule with u^2 and u^3 following a similar construction with v_2 and v_3 the spatial velocities. By enforcing time-like normalization $\mathbf{u}\cdot\mathbf{u} = -1$, u^t can be found to be

$$u^t = \frac{e^{-\nu}}{\sqrt{1-v^2}}, \tag{2.33}$$

where

$$v^2 = e^{2\psi-2\nu}(\Omega-\omega)^2 + e^{2\mu_2-2\nu}(v_2)^2 + e^{2\mu_3-2\nu}(v_3)^2. \tag{2.34}$$

Now, in order order to find the four velocity components $u^{\hat{\beta}}$ in a local inertial frame we must find the orthonormal components $(\mathbf{e}_\alpha)^{\hat{\beta}}$ of the coordinate basis vectors, and then calculate the orthonormal four velocity components by [1]

$$u^{\hat{\beta}} = u^\alpha(\mathbf{e}_\alpha)^{\hat{\beta}}. \tag{2.35}$$

To find the needed components of the coordinate basis we begin with the arbitrary choice $\mathbf{e}_\phi = A\mathbf{e}_{\hat{\phi}}$ and

$$\mathbf{e}_\phi \cdot \mathbf{e}_\phi = A^2\mathbf{e}_{\hat{\phi}}\cdot\mathbf{e}_{\hat{\phi}} = A^2, \tag{2.36}$$

where the last equality follows from Eq 2.16, and this expression implies $A = e^\psi$ which determines the orthonormal components of the ϕ basis vector. Now assume

that $\mathbf{e}_t = B\mathbf{e}_{\hat{t}} + C\mathbf{e}_{\hat{\phi}}$, and so the coordinate time basis vector is assumed to be a linear combination of the orthonormal azimuthal and time basis vectors. Follow the same process and use the orthogonality of $\eta_{\mu\nu}$. From this procedure, the orthonormal components of the coordinate basis are found to be

$$(\mathbf{e}_t)^{\hat{\alpha}} = \begin{pmatrix} e^{\nu} \\ -\omega e^{\psi} \\ 0 \\ 0 \end{pmatrix}, \ (\mathbf{e}_\phi)^{\hat{\alpha}} = \begin{pmatrix} 0 \\ e^{\psi} \\ 0 \\ 0 \end{pmatrix}, \ (\mathbf{e}_2)^{\hat{\alpha}} = \begin{pmatrix} 0 \\ 0 \\ e^{\mu_2} \\ 0 \end{pmatrix}, \ (\mathbf{e}_3)^{\hat{\alpha}} = \begin{pmatrix} 0 \\ 0 \\ 0 \\ e^{\mu_3} \end{pmatrix}. \quad (2.37)$$

From Eq 2.37 and Eq 2.35,we can calculate the azimuthal component of the particle's four velocity in the local inertial frame to be

$$u^{\hat{\phi}} = \frac{e^{\psi-\nu}}{\sqrt{1-v^2}}(\Omega - \omega). \quad (2.38)$$

The other components are straightforward to find, but it is this component that illustrates the effect of inertial frame dragging. A particle that is at rest in a local inertial frame, where $u^{\hat{\phi}} = u^2 = u^3 = 0$, will acquire a non-zero coordinate angular velocity Ω, from Eq 2.38, in the same direction of the matter source's rotation ($\Omega = \omega$). Hence, even though a particle is at rest in a local inertial frame, it acquires an angular velocity because the inertial frame is dragged by rotation.

This discussion is based on the presentation in [13], but takes a more direct route, opting to instead find the orthonormal components $(\mathbf{e}_\alpha)^{\hat{\beta}}$ of the coordinate basis vectors (relatively easy) rather than both the covariant and contravariant coordinate components of the orthonormal basis vectors (a bit more tedious). For further discussion and the proof of Eq 2.31, see [13].

Effect on test spins

Now, turning to the effect of this rotation on test spins, why does inertial frame dragging cause gyroscopes to precess? Explicitly showing the effect of rotation on test spins analytically, via Eq 2.29, even for a simple rotating metric provides little illumination of the behavior. In lieu of a derivation of this behavior, I provide an argument from fluid mechanics to describe the expected behavior and how inertial frame dragging actually influences spin in Fig 2.4 (this argument is found in [12] and is attributed to Schiff, and turns out to be accurate for spacetime).

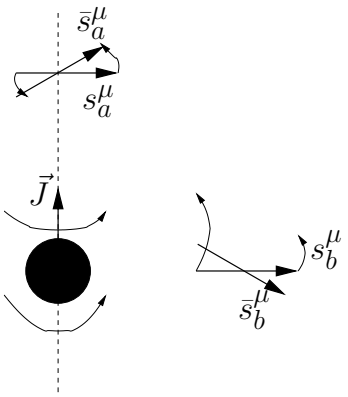

Figure 2.4: Consider a spinning sphere with angular momentum $\vec{J}$ in a viscous fluid. The rotation of the sphere creates currents in the fluid and the fluid is "dragged" by the motion of the sphere. The currents are denoted by curved arrows where longer arrows are stronger currents. Visualizing the spin vectors as little rods it can be seen that along the axis of rotation the s_a^μ vector is dragged in the direction of the rotating body, but the vector in the equatorial plane, s_b^μ, rotates opposite the rotating body because the stronger currents are closer to the rotating body and so the tip is dragged less and the net effect is rotation in the opposite direction. The dragged spin vectors are denoted by bars.

2.5.1 Frames of reference

There are actually three frames involved in the discussion of precession: the frame composed of the orthonormal tetrad carried by an observer with arbitrary acceleration ($\mathbf{e}_{\alpha\prime}$) which *is* Fermi-Walker transported, the local coordinate system of the accelerated observer ($\mathbf{e}_{\hat{\alpha}}$) which *is not* Fermi-Walker transported and the frame in which the distant stars are at rest [12]. For discussions unconcerned with rotation in spacetime, the distinctions can be a little pedantic, but as our discussion will be heavily focused on the precession, orientation of gyroscopes the distinctions are essential to understand.

There are three conditions that are imposed on the tetrad. The first two are that they must remain orthonormal and constitute a rest frame for the observer [12]. Both the tetrad and the local inertial coordinates satisfy these conditions as both $\mathbf{e}_{\mu\prime} \cdot \mathbf{e}_{\nu\prime}$ and $\mathbf{e}_{\hat{\mu}} \cdot \mathbf{e}_{\hat{\nu}}$ are equivalent to $\eta_{\mu\nu}$ (remain orthonormal) and they are both rest frames (although the local inertial frame is only for a single instant). The third condition is why the distinction becomes relevant: the orthonormal tetrad that an observer carries with them is non-rotating, by definition. The very concept of what defines "nonrotating" is actually not trivial, but can be interpreted in the intuitive sense as non-rotation of the three spacial vectors (see [12] for more complete description). The tetrad cannot rotate, but the local inertial frames can (and actually do as described in Chap 2.5), and it is with respect to these two frames that precession is considered. Furthermore, consider an observer returning to a particular spacial coordinate (in a circular orbit for instance), the spin vector of a gyroscope that the observer carried with them was Fermi-Walker transported along the orbit, but the orientation of a gyroscope in a local inertial comoving frame was not Fermi-Walker transported, so when the observer returns there is no reason to expect the two spins to agree (in fact they, in general, will not which will be demonstrated in 3.1.2). Therefore, we see this distinction is crucial for interpretations of precession: precession is the discrepancy measured between the spin vector the gyroscope carries with it and the instantaneous local inertial comoving frame of another observer "flying overhead" at that instant. This comoving frame is related by a Lorentz boost to the frame in which distant stars are at rest which is why it is claimed the gyro will precess with respect to distant stars [1].

2.6 The Einstein Field Equations and the Stress-energy Tensor

The full theory and formalism of stress-energy will not be introduced, but the necessities needed to understand just what it *means* for a geometry to solve Einstein's equations or if a geometry has physical matter sources will be discussed.

Before introducing the Einstein equations, consider the definition for the covariant derivative of a vector [1],

$$\nabla \mathbf{v}^{\beta}_{\alpha} = \nabla_{\alpha} v^{\beta} = \frac{\partial v^{\beta}}{\partial x^{\alpha}} + \Gamma^{\beta}_{\alpha\gamma} v^{\gamma}. \tag{2.39}$$

In brief, this definition is motivated by the fact that a derivative of a vector involves the difference of vectors at two nearby points, then taking the limit of the separation to 0. However, the two vectors "live" in different tangent spaces and so they cannot be directly subtracted in an arbitrarily curved space; they must be transported correctly from one point to the other first which the Γ's in Eq 2.39 guarantee [1], by encoding all the information about the variation of the bases. So in addition to the derivative term in Eq 2.39, the connection coefficients make an expected appearance. In summary, Eq 2.39 defines the correct derivative of a vector.

Riemann curvature

Gravity vanishes in local inertial freely-falling frames and so there is no way for such observers to *feel* the effects of gravity. Thus, the only way to measure the gravity created by the curvature of spacetime is to measure the relative accelerations of test particles [12]. In flat space, nearby freely-falling particles do not accelerate relative to each other because the Γ's in Eq 2.25 vanish, and so this would constitute a test that would verify that the spacetime is flat. But how does one actually calculate relative accelerations when the curvature is non-trivial? Following the idea that curvature must directly be tied to relative accelerations, we calculate the second covariant derivative (the acceleration) of the separation vector χ between two nearby geodesics along the four velocity $\mathbf{u}$ (denoted $\nabla_{\mathbf{u}}$)[1]

$$(\nabla_{\mathbf{u}} \nabla_{\mathbf{u}} \chi)^{\alpha} = -R^{\alpha}_{\beta\gamma\delta} u^{\beta} \chi^{\gamma} u^{\delta}, \tag{2.40}$$

where $\mathbf{R}$ is a rank-four tensor called the Riemann curvature tensor which is an expression of sums and derivatives of the connection coefficients. The components can

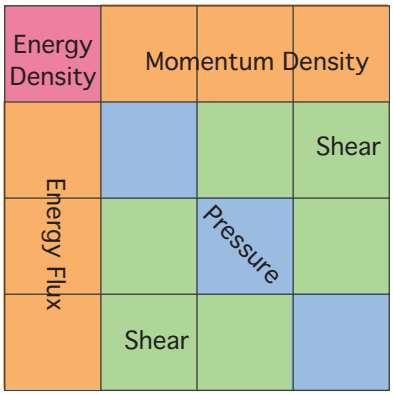

Figure 2.5: Summary of the components of the Stress-Energy-Momentum Tensor.

be explicitly found from working out the expressions of the covariant derivatives [1]). The Riemann tensor provides the necessary measure of curvature.

Stress-Energy and the Einstein equations

As we would like to find a relation between matter and curvature (Eq 2.40 is the curvature), we require an object that contains all the information about the properties of the matter of a system: its total mass, energy, momentum and any pressures or shear stresses. That object is the second-rank tensor known as the stress-energy tensor $T^{\mu\nu}$ with components summarized in Fig 2.5. For example, the T^{00} component is the energy density and for realistic matter it must be positive. A negative energy density requires exotic matter and is needed in many wormhole geometries.

From the Riemann curvature tensor, we define the Ricci tensor($R_{\mu\nu}$):

$$R^{\alpha}_{\mu\alpha\nu} = R_{\mu\nu}, \tag{2.41}$$

and the Ricci scalar R via

$$R = R^{\alpha}_{\alpha}. \tag{2.42}$$

As we now have two second rank tensors, we can form a tensor equation where a measure of curvature is on one side and a measure of matter and energy on the other: a way to relate matter to spacetime curvature, relating matter and gravity. The equation ends up taking the form [1]

$$R_{\alpha\beta} - \frac{1}{2} g_{\alpha\beta} R = 8\pi T_{\alpha\beta} \tag{2.43}$$

which are the Einstein equations. For regions of spacetime where there is no matter ($T_{\alpha\beta} = 0$) then we have the vacuum Einstein equations

$$R_{\alpha\beta} = 0. \tag{2.44}$$

The Ricci and stress-energy tensors are both symmetric and so they constitute a set of ten non-linear differential equations and so analytical solutions can only be hoped for by assuming a certain degree of symmetry. This process will be described for the two spacetime metrics considered in this paper in Chap 4.1 and Chap 4.2.

2.7 Closed Timelike Curves

In short, a CTC is any timelike closed curve in spacetime [4]. What is meant by this is take any point in spacetime, draw a closed curve that ends back at that point and if the four velocity is timelike at all points along the curve then it is a closed timelike curve. The easiest way to see this is to consider an axisymmetric metric[17]

$$ds^2 = -A(r)dt^2 + 2B(r)d\phi dt + C(r)d\phi^2 + D(r)(dr^2 + dz^2), \tag{2.45}$$

and hold all the coordinates constant except the azimuthal coordinate and the length squared of the azimuthal curve is $s^2 = C(r)4\pi^2$. If $C(r)$ is negative then the curve is *timelike* and by the periodic nature of the azimuthal coordinate and the preceding discussion, *closed*. Why this is unusual is that coordinates that are periodic are not usually able to become timelike without any rotation. A CTC would "allow accelerated observers to return to their starting points with no coordinate time having elapsed" [15] which we see here because t becomes constant. Other cases where other coordinates become timelike (like in the Schwarzschild case for inside the event horizon where the r coordinate becomes timelike) can have odd reversed temporal behavior, but if the coordinate is not periodic (such as in the Schwarzschild case), it does not constitute a CTC and could not be possibly exploited as a time machine or provoke a causality violation.

The importance of geodesics in this discussion is that it is hard to verify that non-geodesic paths (paths where the observer is not freely falling) are physical, but geodesic paths are automatically physical[15]. For this reason, this paper is primarily concerned with simulations of time-like geodesic paths.

As mentioned, a primary goal of this paper is to explore the physical or non-physical mechanism by which CTC's arise. As Andréka et. al. note [16], the standard

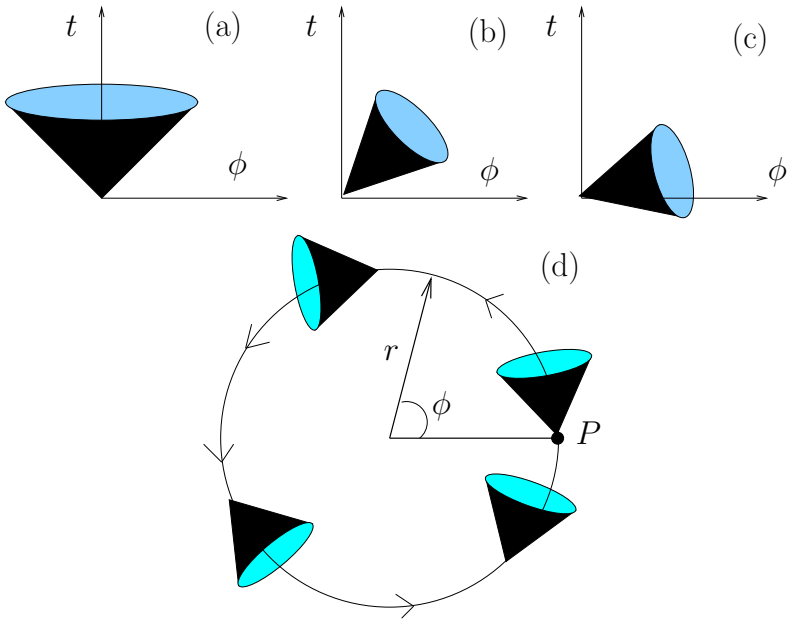

Figure 2.6: (a) is a flat space light cone and (b) shows the same light cone that has been distorted and tipped over by inertial frame dragging induced by spacetime rotation and could be a light cone in the ergosphere of the Kerr geometry (a region of spacetime where an observer could not remain at a constant ϕ even with arbitrarily powerful rockets [1] due to the extreme frame dragging). (c) shows an exceptionally strong region of frame dragging that has tipped the light cones over so far that it now permits the observer to travel along a curve of constant t and, as shown in (d), meet themselves at P with no coordinate time having elapsed. (d) is a simple example of a CTC created by the frame dragging of rotating matter in the expected way: the time traveler must travel in the direction of the rotating matter, as that is the way the light cones tip.

explanation for the creation of closed timelike curves, in the literature, is that the frame dragging effect of rotating matter drags the light cones to the extent that the azimuthal coordinate becomes timelike, as seen in Fig 2.6. The authors mention this would imply that the time traveler must co-rotate with the matter, but this is not what happens in their paper; they posit that time travelers must counter-rotate with the rotating matter of their time-machine in order to follow CTC's. This claim casts doubt on the claim that it is solely due to rotating matter and frame dragging that CTC's are created; there appears to be an unknown secondary mechanism that causes the light cones to tip, counter-intuitively, in the other direction. If this is the case, a possible way to probe this would be to see if it has any precessional effect.

Chapter 3

Quantifying Gyroscope Motion in Curved Spacetime

3.1 Gyroscope Motion in The Schwarzschild Geometry

The Schwarzschild metric describes the metric outside a massive spherical body (a star, black hole, etc.) and is written [1]

$$\begin{aligned} ds^2 &= -\left(1-\frac{2M}{r}\right)dt^2+\left(1-\frac{2M}{r}\right)^{-1}dr^2 \\ &+ r^2(d\theta^2+\sin^2\theta d\phi^2), \end{aligned} \tag{3.1}$$

where the Schwarzschild coordinates

$$x^\mu = \begin{pmatrix} t \\ r \\ \theta \\ \phi \end{pmatrix} , \tag{3.2}$$

have been adopted.

Although the gyroscope equation, Eq 2.29, becomes incredibly complicated quickly for non-trivial geometries, an analytical solution is tractable for the Schwarzschild case. This provides a check on the numerical simulations and also expounds on the method for calculating the precession of gyroscopes.

3.1.1 The four velocity for Schwarzschild circular orbits

In order to solve the gyroscope equation, the four velocities for the gyroscopes must be found. Following the Lagrangian formalism, we start with the Lagrangian [11]

$$\mathcal{L} = g_{\mu\nu}\dot{x}^{\mu}\dot{x}^{\nu} \tag{3.3}$$

to find the orbits, with $\theta = \pi/2$ (equatorial) and $r =$ constant (circular). The Euler-Lagrange equations yield:

$$\begin{aligned} \left(1 - \frac{2M}{r}\right)\dot{t} &= e, \\ r^2\dot{\phi} &= \ell, \end{aligned} \tag{3.4}$$

where e and ℓ are constants (energy and angular momentum, respectively) and the time-like normalization gives

$$-\left(1 - \frac{2M}{r}\right)\dot{t}^2 + r^2\dot{\phi}^2 = -1. \tag{3.5}$$

From these, the constants in Eq 3.4 can be found to be [11]

$$\ell^2 = \frac{Mr^2}{r - 3M}, \tag{3.6}$$

$$e = \frac{\left(1 - \frac{2M}{r}\right)}{\left(1 - \frac{3M}{r}\right)^{1/2}}. \tag{3.7}$$

Therefore, $\dot{t} = u^0 = (1-3M/r)^{-1/2}$ and $\dot{\phi}^2 = (M/r^2)(r-3M)^{-1}$, and so a test body's four velocity is given by

$$u^{\alpha} = u^0 \begin{pmatrix} 1 \\ 0 \\ 0 \\ \Omega \end{pmatrix}, \tag{3.8}$$

for circular orbits, where $\Omega = (M/r^3)^{1/2}$.

3.1.2 Schwarzschild geodetic precession

From Eq 3.8, the orientation of gyroscopes for an orbiting test body can be found using Eq 2.29. From $\boldsymbol{s} \cdot \boldsymbol{u} = 0$,

$$s^t = R^2\Omega\left(1 - \frac{2M}{R}\right)s^{\phi} \tag{3.9}$$

because $s^\theta = 0$ as it initially points in the equatorial plane and thus must remain 0 by symmetry of the equatorial plane for all time. Solving the gyroscope equation for the remaining s^r and s^ϕ results in two coupled differential equations where one can be substituted into the other to yield a second order equation that has the simple harmonic oscillator form with frequency [1]

$$\bar{\Omega} = \left(1 - \frac{3M}{R}\right)^{1/2} \Omega. \tag{3.10}$$

Choosing the initial spin orientation to be radial with the spin normalized to 1 and writing in terms of coordinate time t (for convenience) gives:

$$\begin{aligned} s^r(t) &= \left(1 - \frac{2M}{R}\right)^{1/2} \cos(\bar{\Omega}t), \\ s^\phi(t) &= -\left(1 - \frac{2M}{R}\right)^{1/2} \left(\frac{\Omega}{\bar{\Omega}R}\right) \sin(\bar{\Omega}t). \end{aligned} \tag{3.11}$$

With $(\mathbf{s} \cdot \mathbf{s})^{1/2} = s_* = 1$, the initial ($t = 0$) spin four vector is $s^\alpha(0) = (0, (1 - 2M/r)^{(1/2)}, 0, 0)$. An orbit is completed in coordinate time $P = 2\pi/\Omega$ and so to get the $\delta\phi$ of geodetic precession per orbit it suffices to find the angle between $s^\alpha(0)$ and $s^\alpha(P)$. The angle θ between two vectors v^μ and w^ν is given by Eq 2.8 and noting that both $s^\alpha(0)$ and $s^\alpha(P)$ have magnitudes of 1 we see

$$\cos\theta = g_{rr} s^r(0) s^r(P), \tag{3.12}$$

where $s^r(P)$ can be found from Eq 3.11 and so

$$\theta = 2\pi \frac{\bar{\Omega}}{\Omega} = 2\pi \left(1 - \frac{3M}{r}\right)^{1/2}. \tag{3.13}$$

After one orbit, the total rotation is $2\pi - \theta$ and we conclude:

$$\Delta\phi_{\text{geodesic}} = 2\pi \left\{1 - \left(1 - \frac{3M}{r}\right)^{1/2}\right\} \tag{3.14}$$

per orbit. See [1] and [11] for more complete discussion.

Therefore, any gyroscope in motion about a massive body will experience precession due entirely to the massive body's curvature of spacetime and is called *geodetic* precession in order to differentiate it from precession due to inertial frame dragging, considered in the following subsection. Eq 3.14 also provides a check for a specific case in the numerical simulations. In Sec 6.2, $\cos\theta$ will be plotted against t or *tau* along a circular orbit which is calculated similarly to Eq 3.12, except more points than just one orbital period will be plotted.

Chapter 4

The Spacetime Metrics Considered

The Kerr black hole and the van Stockum cylinder exhibit non-trivial CTC's because they are caused by the dragging of inertial frames [4]. CTC's can be artificially created by unusual choices of coordinates, but the Kerr and van Stockum spacetimes are unique because they can't be removed by coordinate methods. Here, we introduce the two spacetimes: the Kerr metric and the van Stockum metric.

4.1 The geometry of the Kerr rotating black hole

In 1963, Roy Kerr discovered the line element describing the spacetime of a rotating spherically symmetric mass with mass M and angular momentum J to be [1]

$$\begin{aligned} ds^2 &= -\left(1-\frac{2Mr}{\rho^2}\right)dt^2 - \frac{4Mar\sin^2\theta}{\rho^2}d\phi dt + \frac{\rho^2}{\triangle}dr^2 + \rho^2 d\theta^2 \\ &+ \left(r^2+a^2+\frac{2Mra^2\sin^2\theta}{\rho^2}\right)\sin^2\theta d\phi^2 \end{aligned} \tag{4.1}$$

with $a \equiv J/M$, $\rho^2 \equiv r^2 + a^2\cos^2\theta$, and $\triangle \equiv r^2 - 2Mr + a^2$.

4.1.1 The derivation of the Kerr black hole

The actual derivation of the Kerr black hole is long and algebraically complicated and is provided in [13]. Here, merely the process will be described. Starting with the general axisymmetric stationary metric, Eq 2.31, and by computing all the necessary derivatives and sums of the metric, we are left to compute the necessary metric functions that satisfy the vacuum Einstein equations, Eq 2.44 [11]. In the non-rotating case (the Schwarzschild metric), one assumes a spherically symmetric metric and it turns out that Eq 2.44 is sufficient to determine the geometry uniquely. However, axisymmetry is less restrictive than spherical symmetry and so, in fact, Eq 2.44 are not enough to uniquely determine a solution [11]. What yields the Kerr solution is enforcing that if an observer is far enough away then the local geometry becomes flat, or as $r \to \infty$, $g_{\mu\nu} \to \eta_{\mu\nu}$. This is reasonable because if the observer is far enough away from the black hole then its gravity should not be noticeable.

4.1.2 Kerr Circular Orbits

The procedure to find the four velocities for the Kerr circular orbits is similar to the discussion in Chap 3.1.1 for the Schwarzschild case, but the algebra is more complicated. The four velocities take the similar form Eq 3.8, but there are actually two values of Ω which correspond to orbits in the direction of the black hole rotation (co-rotating) and opposite the rotation (counter-rotating) which are given by[13]

$$\Omega = \frac{\mp\sqrt{Mu^3}}{1 \mp a\sqrt{Mu^3}}, \tag{4.2}$$

where $u = 1/r$. In this paper, only co-rotating orbits are considered.

4.2 The geometry of the van Stockum cylinder

In 1936, van Stockum attained a solution for the field of a rapidly rotating cylinder where centrifugal forces balance the gravitational effects. The metric for such a cylinder is expressed as [2] [3]

$$ds^2 = H(r)(dr^2 + dz^2) + L(r)d\phi^2 + 2M(r)d\phi dt - F(r)dt^2. \tag{4.3}$$

If ω is the angular velocity of the cylinder and a is the radius of the cylinder, then the functions for the metric, for the parameter range in which $\omega a > 1/2$ and the region outside the cylinder, are

$$\begin{aligned} H &= e^{-\omega^2 a^2}(r/a)^{-2\omega^2 a^2}, \\ L &= \frac{ar\sin(3\beta+\gamma)}{2\sin(2\beta)\cos(\beta)}, \\ M &= \frac{r\sin(\beta+\gamma)}{\sin(2\beta)}, \\ F &= \frac{r\sin(\beta-\gamma)}{a\sin(\beta)}, \end{aligned} \tag{4.4}$$

where

$$\begin{aligned} \gamma &= (4\omega^2 a^2 - 1)^{1/2}\ln(r/a) \\ \beta &= tan^{-1}(4\omega^2 a^2 - 1)^{1/2}. \end{aligned} \tag{4.5}$$

4.2.1 The derivation of the van Stockum cylinder

The derivation of the van Stockum dust cylinder is similar to the Kerr solution in Sec 4.1.1, but because van Stockum considers an infinite cylinder we cannot let the field tend to flat space at infinity, it is not asymptotically Minkowskian, and so an additional constraint must be imposed to uniquely determine the field and van Stockum assumes that the stress-energy of the cylinder is that of incoherent matter, $T^{\alpha}_{\beta} = \mu u^{\alpha} u_{\beta}$, where μ is the density of particles and u^{α} is the four-velocity of the matter. The process that van Stockum takes is to first find the correct form of the stress-energy for dust particles rotating with a constant angular velocity in a co-rotating frame (the interior solution), and then matches it to the vacuum solution (the exterior solution), using Eq 2.44.

4.2.2 Circular timelike orbits and CTC's

Steadman, in [15], found four velocities for CTC's and circular orbits along which coordinate time runs backward and also circular orbits that close and along which no coordinate time advances (the CTC's). The metric functions in Eq 4.3 have no

coordinate t, ϕ, or z dependence we can associate with each a conserved constant which are, from the Euler-Lagrange equations, Eq 2.24,

$$\begin{aligned} p_t &= F\dot{t} - M\dot{\phi}, \\ p_\phi &= -M\dot{t} - L\dot{\phi}, \\ p_z &= H\dot{z}. \end{aligned} \tag{4.6}$$

Steadman then considers a timelike path in the region where $g_{\phi\phi} < 0$, from Chap 2.7 discussion, this is where CTC could occur, rearranges the Eqs 4.6 and assumes circular orbits: $\ddot{r} = 0$ and $\dot{r} = 0$. He then writes the t and ϕ components of the four velocity for a circular timelike orbit in the van Stockum metric, in terms of p_t [15]:

$$\begin{aligned} \dot{t} &= \frac{a\sin(2\beta + \frac{1}{2}\log(\frac{r}{a})\tan\beta)}{2a\cos\beta\sin(\beta - \frac{1}{2}\log(\frac{r}{a})\tan\beta)}\, p_t \\ \dot{\phi} &= -\frac{\sin(\frac{1}{2}\log(\frac{r}{a})\tan\beta))}{r\sin(\beta - \frac{1}{2}\log(\frac{r}{a})\tan\beta)}\, p_t \end{aligned} \tag{4.7}$$

Note that the zeros of the $\dot{t}$ equation in Eq 4.7 correspond to paths where t =constant and so are CTC's. Likewise, radial coordinates where $\dot{t} < 0$ correspond to circular orbits where coordinate time runs backward. These expressions provide the necessary initial four velocities to plot the paths of timelike particles in exotic circular orbits (CTC's and causality violating) and this paper seeks to compare the precession of gyroscopes in these strange orbits to the more familiar orbits of the Kerr and Schwarzschild geometries.

As mentioned, because it is not asymptotically flat it does not appear that the van Stockum cylinder is realistic, but Tipler in [2] argues that the classical Newtonian analogue also has a gravitational field that diverges and so it could hold for realistic cylinders. In addition, there are CTC's inside the horizon of the Kerr metric [9] and so it is hypothesized that a sufficiently large finite cylinder could have CTC's in the exterior vacuum.

Chapter 5

Numerical Methods

In this chapter, we outline the numerical methods implemented and various numerical checks. The bulk of the numerical methods involve numerically solving the geodesic and gyroscope equation (Eq 2.25 and Eq 2.29, respectively) with a 4th order Runge-Kutta routine, outlined in Chap 5.1, written in C++. Example simulations and parameters are discussed in Chap 5.2.

5.1 Fourth Order Runge-Kutta (RK4)

As Eq 2.25 is a set of four second order ordinary differential equations it can be written as a set of eight first order equations via the identification Eq 2.22 and becomes, explicitly writing in dependent variables:

$$\frac{du^{\alpha}(\tau)}{d\tau} + \Gamma^{\alpha}_{\beta\gamma}(x^{\mu}(\tau))u^{\beta}(\tau)u^{\gamma}(\tau) = 0, \tag{5.1}$$

$$u^{\mu}(\tau) = \frac{dx^{\mu}(\tau)}{d\tau}. \tag{5.2}$$

In addition, the initial conditions must satisfy:

$$\begin{aligned} \boldsymbol{u}\cdot\boldsymbol{u} = g_{\mu\nu}u^{\mu}u^{\nu} &= -1, \\ \boldsymbol{s}\cdot\boldsymbol{u} &= 0, \\ \sqrt{\boldsymbol{s}\cdot\boldsymbol{s}} &= s_{*}, \end{aligned} \tag{5.3}$$

where s_* is a constant and is set to 1. As u^μ and s^μ (the gyroscope equation is also integrated and is included with Eqs 5.1 and 5.2) are parallel transported during the integration, if the constraints are satisfied by the initial conditions they will remain satisfied at all points along the world line.

The general form of ordinary differential equations to be integrated is

$$\frac{d\boldsymbol{\zeta}}{d\tau} = \mathbf{f}(\boldsymbol{\zeta}(\tau), \tau), \tag{5.4}$$

where $\boldsymbol{\zeta}$ is a state vector that has all the components of the position, four velocity and the spin (12 components). We note that for the four velocity and spin vector components the right hand side of Eq 5.4 involves the geodesic equation and gyroscope equation, respectively. The general discretization of the system of differential equations, Eq 5.4, into a Runge-Kutta step is[7]

$$\boldsymbol{\zeta}(\tau + \Delta\tau) = \boldsymbol{\zeta}(\tau) + \frac{1}{6}\Delta\tau(\mathbf{F}_1 + 2\mathbf{F}_2 + 2\mathbf{F}_3 + \mathbf{F}_4), \tag{5.5}$$

where the $\mathbf{F}$'s are given by the usual Runge-Kutta formulas, see [7]. To illuminate this discussion, we provide the discretization of the four velocity equation. The Runge-Kutta formulas are, noting the coordinate dependence of the Γ's:

$$\begin{aligned}
F_1^\alpha &= -\left\{\Gamma^\alpha_{\beta\gamma}(x^\mu)\right\} u^\beta u^\gamma, \\
F_2^\alpha &= -\left\{\Gamma^\alpha_{\beta\gamma}(x^\mu + (1/2)\Delta\tau F_1^\mu)\right\} (u^\beta + (1/2)\Delta\tau F_1^\beta)(u^\gamma + (1/2)\Delta\tau F_1^\gamma), \\
F_3^\alpha &= -\left\{\Gamma^\alpha_{\beta\gamma}(x^\mu + (1/2)\Delta\tau F_2^\mu)\right\} (u^\beta + (1/2)\Delta\tau F_2^\beta)(u^\gamma + (1/2)\Delta\tau F_2^\gamma), \\
F_4^\alpha &= -\left\{\Gamma^\alpha_{\beta\gamma}(x^\mu + \Delta\tau F_3^\mu)\right\} (u^\beta + \Delta\tau F_3^\beta)(u^\gamma + \Delta\tau F_3^\gamma).
\end{aligned}$$

The components of the $\mathbf{F}$'s actually serve double-duty as there are components that correspond to both the coordinates and the four velocities, but the context in which they appear in Eq 5.6 should be clear. These formula are then substituted into the general Runge-Kutta formula for the four velocity step,

$$\boldsymbol{u}(\tau + \Delta\tau) = \boldsymbol{u}(\tau) + \frac{1}{6}\Delta\tau(\mathbf{F}_1 + 2\mathbf{F}_2 + 2\mathbf{F}_3 + \mathbf{F}_4). \tag{5.6}$$

The position and spin four vector integration is similar and, once the solutions $\boldsymbol{s}(t)$ and $\boldsymbol{s}(\tau)$ are found, the precession angles $\cos\theta(t)$ or $\cos\theta(\tau)$ are calculated via Eq 2.8. All that remains is to calculate the Γ's for the considered geometry and these are provided in A.1 for the Kerr and van Stockum geometries. The C++ code for the integration of the van Stockum cylinder is provided in A.2.

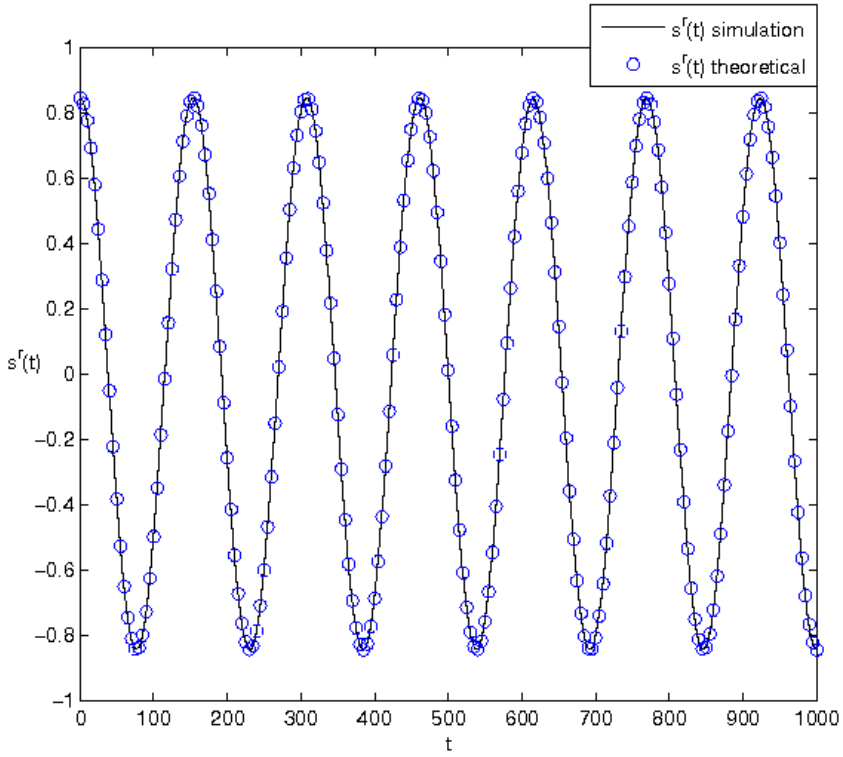

Figure 5.1: Plot of $s^r(t)$ for Schwarzschild circular orbit of r =6.5 is compared with the theoretical expression Eq 3.11.

5.2 Simulations and Parameters

In all simulations, M the mass of the black hole (both Kerr and Schwarzschild) is set to 1. J, the angular momentum for a Kerr black hole is set to 0.9, and ω, the angular frequency of the van Stockum cylinder is also set to 0.9. The radius of the van Stockum cylinder, a, is 1. All simulations are with a tau step of $\Delta\tau = 0.01$.

Simulations of the dependence of s^r and s^ϕ on t are provided in Figs 5.1 and 5.2 for Schwarzschild black hole circular orbits of $r = 6.5$. The plots are compared with the respective theoretical predictions in 3.11 to validate the numerical code. A plot of the cosine of the angle θ between the spin four vector s^α and the initial radially pointing spin vector $s^\alpha(0)$ as a function of time is provided in Fig 5.3 with the theoretical prediction, and it is these types of plots that will be used to analyze the precession of gyroscopes.

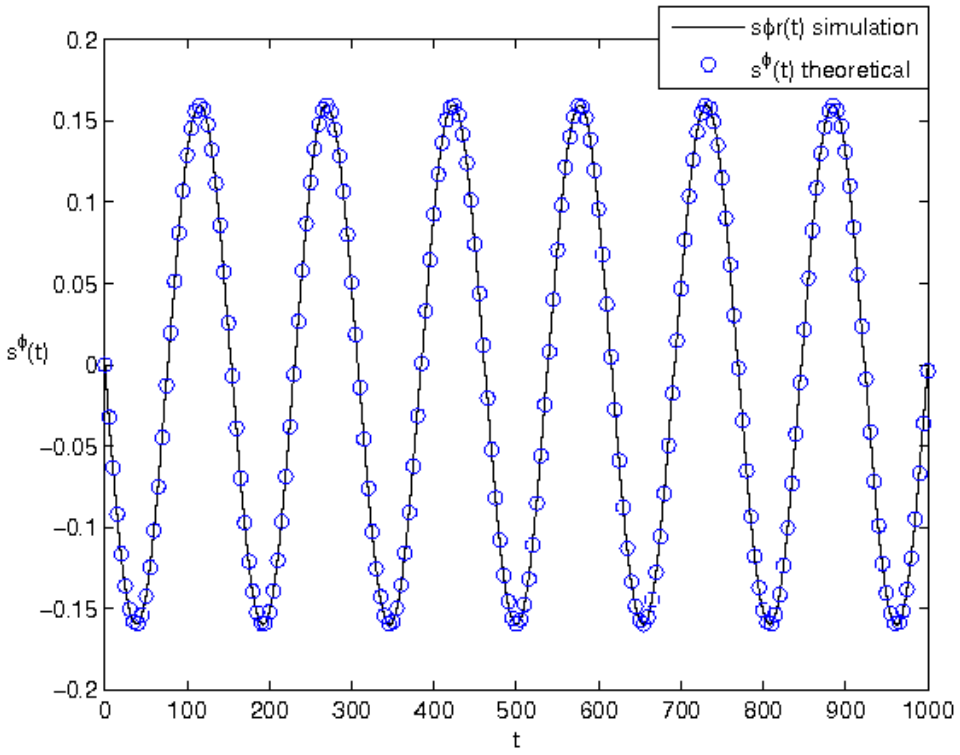

Figure 5.2: Plot of $s^{\phi}(t)$ for Schwarzschild circular orbit of r =6.5 is compared with the theoretical expression Eq 3.11

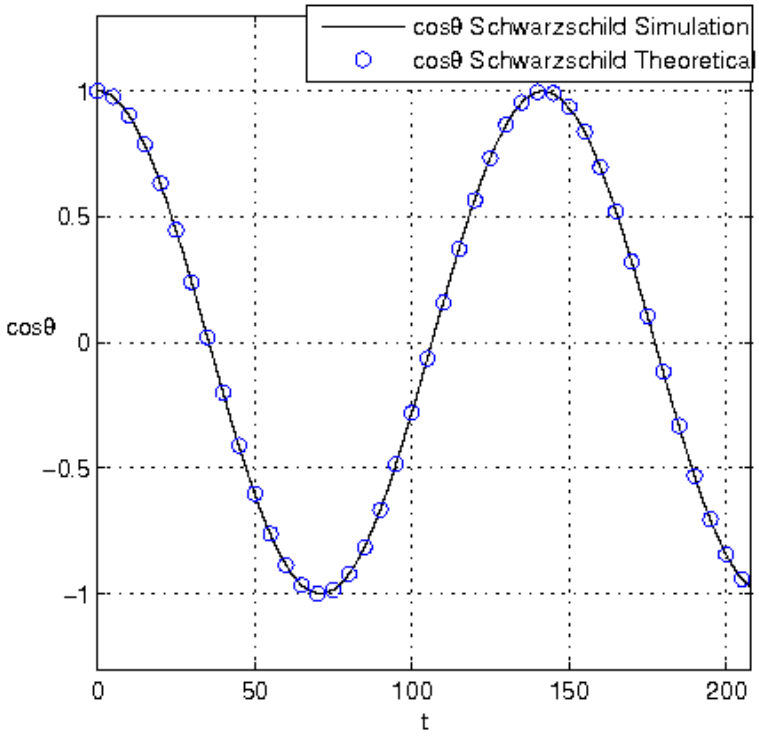

Figure 5.3: Plot of $\cos\theta(t)$ where $\theta(t)$ is the angle between $s^\alpha(t)$ and $s^\alpha(0)$. Here, $r = 6.5$.

Chapter 6

Results

A goal of this paper is to better understand the strange temporal behavior of particle geodesics for the van Stockum cylinder which are presented in Sec 6.1. Results concerned with the processions of gyroscopes are presented in Sec 6.2.

6.1 van Stockum Cylinder Geodesics

van Stockum cylinder geodesics are shown to verify that the four velocities in Eq. 4.7 do, in fact, yield circular orbits in Figs 6.1 and 6.2 which show the same forward time oriented circular timelike orbit of $r = 647.512$. This radius was chosen because it has a circumference length of $6.5(2\pi)$ which coincides with a Schwarzschild orbit of $r = 6.5$, and so will be used for comparison. An example of a CTC is provided in Fig 6.3 for $r = 4.82713$, a zero of Eq 4.7, and so it is expected to be a CTC. Analysis is done exclusively on circular orbits because they are more natural to consider precession on, in order to offer a comparison between the Schwarzschild, Kerr and van Stockum geometries, and provide a simple example of a CTC; however, the van Stockum geometry does create more complicated causality violating "flower petal" orbits as shown in Figs 6.4 and 6.5. Better understanding of these orbits, their symmetry and where they occur, and ways to find ones that close (becoming CTC's) is a topic of future work.

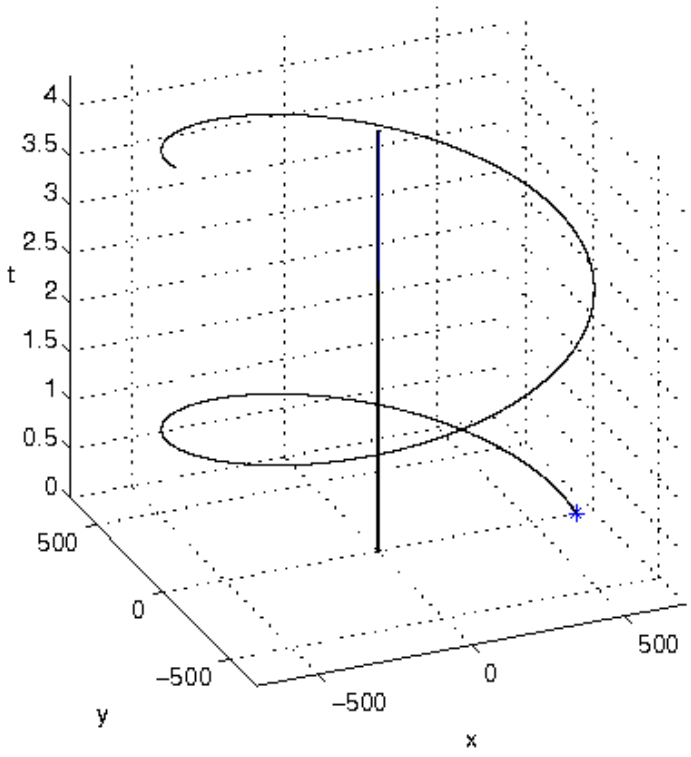

Figure 6.1: An xyt plot (z suppressed) of a forward time oriented timelike circular orbit geodesic in the van Stockum metric of $r = 647.512$, $p_t = 20.1955$ and proper circumference length $6.5(2\pi)$, and so the orbit can be directly compared to the Kerr and Schwarzschild orbits of the same circumference.

6.2 Precession of Gyroscopes

The precession of gyroscopes for orbits in the Kerr rotating black hole and non-rotating Schwarzschild black hole are shown as a function of coordinate time in Fig 6.6 and proper time in Fig 6.7 for orbits of a common circumference length $(2\pi)6.5$, and both figures show the effect of inertial frame dragging. The reason different radii are chosen to make the comparison is that the r coordinate is different for the Schwarzschild and Kerr solutions (Schwarzschild and Boyer-Lindquist coordinates, respectively), so a comparison is made between obits that have the same invariant circumferential distance. Also, the van Stockum r coordinate is different as well which is why Fig 6.8 is at $r = 647.512$. Although this radius is huge (when naively compared to the preceding Schwarzschild and Kerr cases), this radius corresponds to an orbit of circumferential distance $(2\pi)6.5$. Therefore, Figs 6.6, 6.7 and 6.8 all are plotted

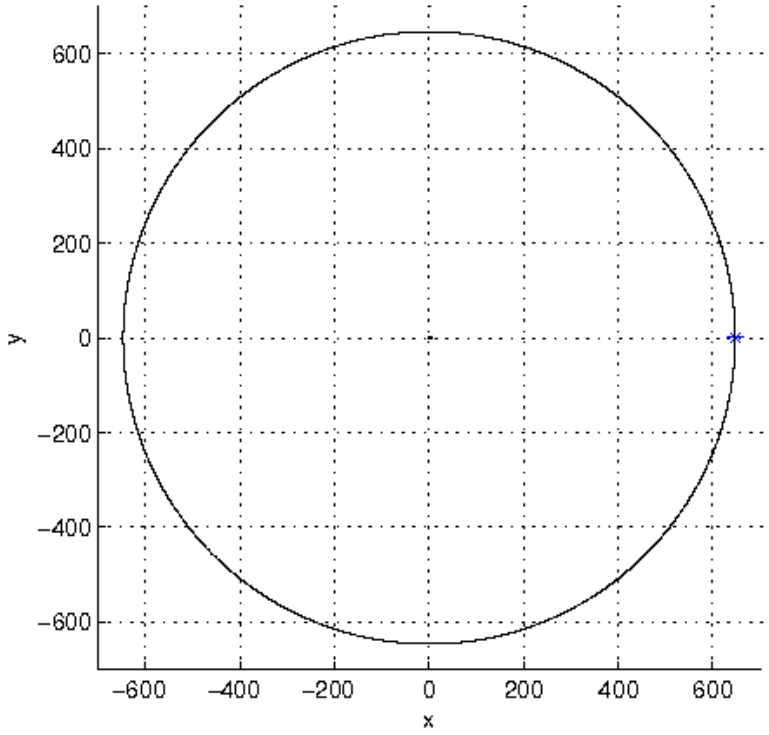

Figure 6.2: An xy projection of Fig 6.1 to show the circular motion.

for orbits that have the same proper circumferential distance.

Gyroscope precession along a CTC in the van Stockum metric is shown in Fig 6.9, and it is clear that the rate at which the gyroscope will precess along the orbit is much greater along the CTC than the preceding cases. The precession along the orbits at radii to the left and right of $r = 4.82713$ is plotted in Fig 6.10 which shows that $r = 4.5$ has even more frame dragging (shifted more to the left) and this is to be expected as, from Fig 6.11, the orbit at $r = 4.5$ is a backward in time oriented circular geodesic, so the light cones have tipped even further over, making the particles travel back in time. The values of p_t for particular circular orbits are collected in Table 6.1.

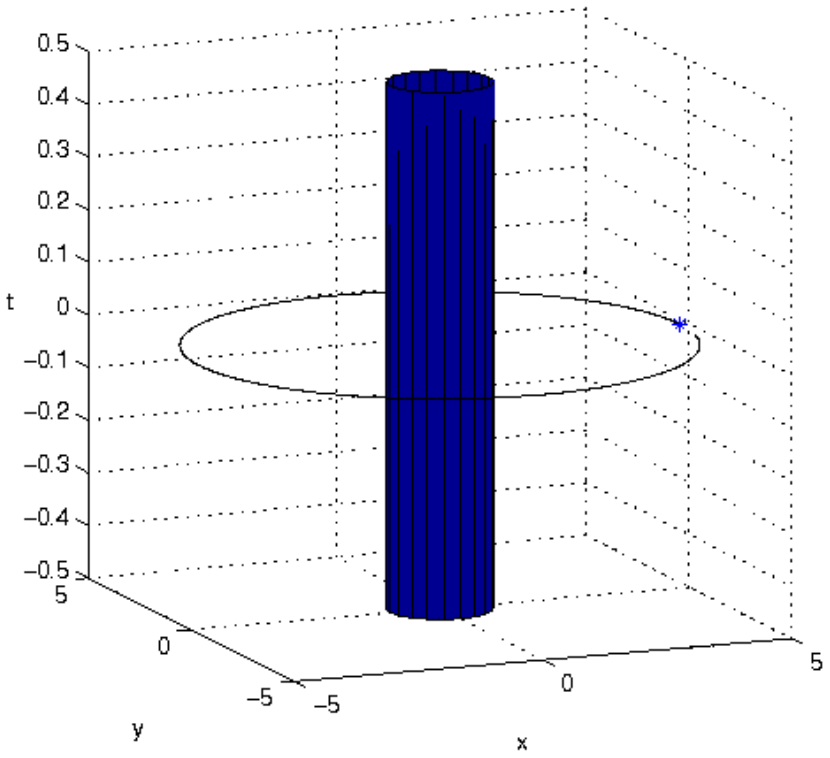

Figure 6.3: An xyt projection of a CTC at $r = 4.82713$. Note that coordinate time does not advance and the particle meets itself at the same place in space at the same place in time. Importantly, the particle does not counter-rotate with the cylinder, seemingly in contrast with [16]

r	p_t	Type
647.512	20.1955	Forward
5.0	0.59377	Forward
4.82713	0.515314	CTC
4.5	0.365565	Backward

Table 6.1: The parameters used for van Stockum circular orbits. The type of circular orbit is also described where Forward denotes forward in time oriented circular orbits, Backward is for orbits where coordinate time runs backward and CTC is a closed timelike curve. The values of p_t where calculated to ensure the timelike normalization $\boldsymbol{u} \cdot \boldsymbol{u} = -1$.

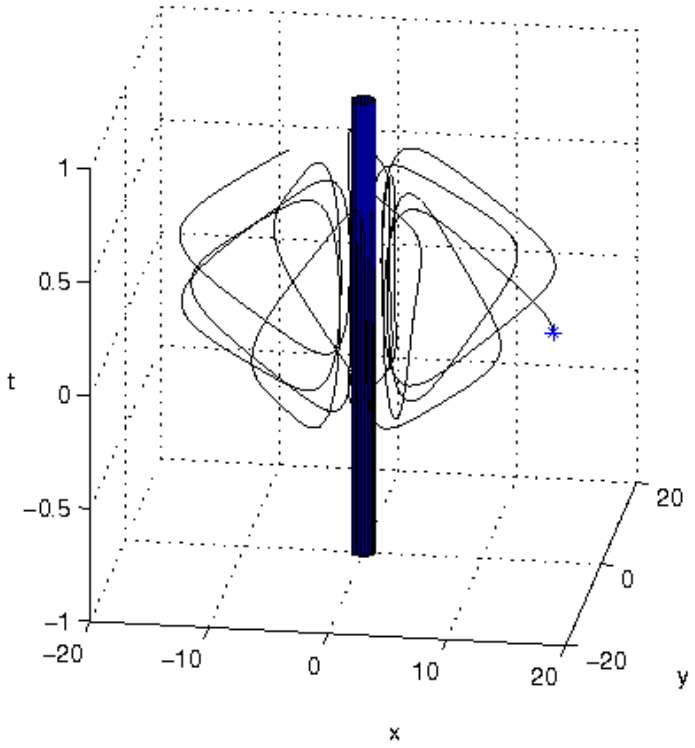

Figure 6.4: An xyz plot of a particle at $r = 17.0$ released from rest (spatial four velocity components set to 0). Shows that the van Stockum solution has more intricate causality violating orbits than circular ones.

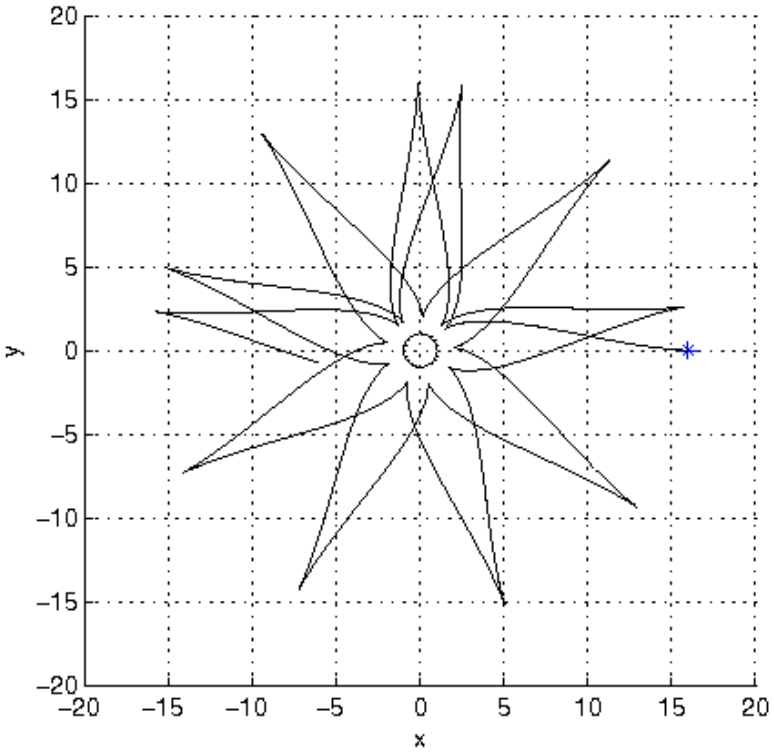

Figure 6.5: An xy projection of Fig 6.4 to show why it is referred to as a "time flower", in this paper.

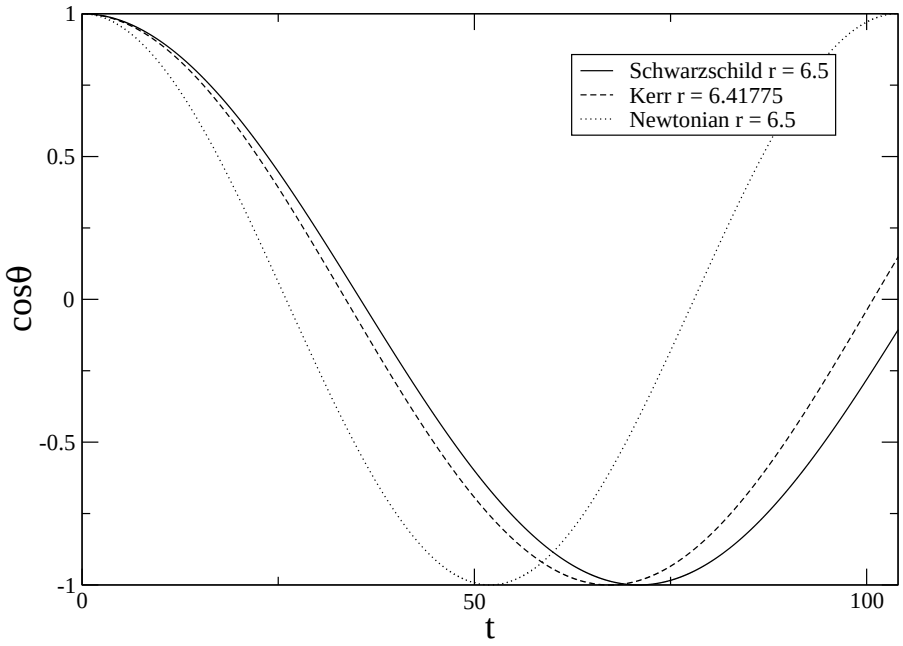

Figure 6.6: Comparison of the precession of gyroscopes for stable circular orbits in the Kerr (co-rotating orbit, $J = 0.9$) and Schwarzschild case for orbit circumference of $6.5(2\pi)$ ($r_{Schwarzschild} = 6.5$, $r_{Kerr} = 6.41775$). Note the effect of inertial frame dragging has caused the Kerr case to have a retarded precession: its precession has been dragged against the precession in the direction of the rotating body, displaying the expected frame dragging effect on spins expected from the discussion in Sec 2.5. The cosine of the angle θ is plotted against coordinate time t that ranges to a period $(2\pi/\Omega)$ of an orbit in the Schwarzschild geometry. The Newtonian curve illustrates the case of no precession.

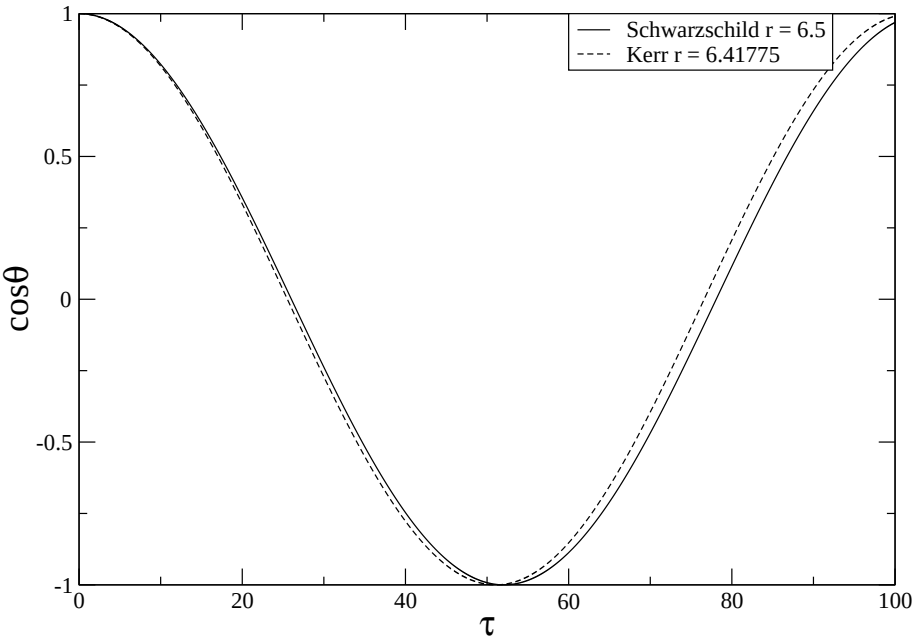

Figure 6.7: The same plot in Fig 6.6, but the cosine of the angle θ is plotted against proper time τ. This is in order to make a comparison to the later case where we will consider a CTC orbit in the van Stockum geometry because coordinate time t will be unusable (it does not advance on a CTC).

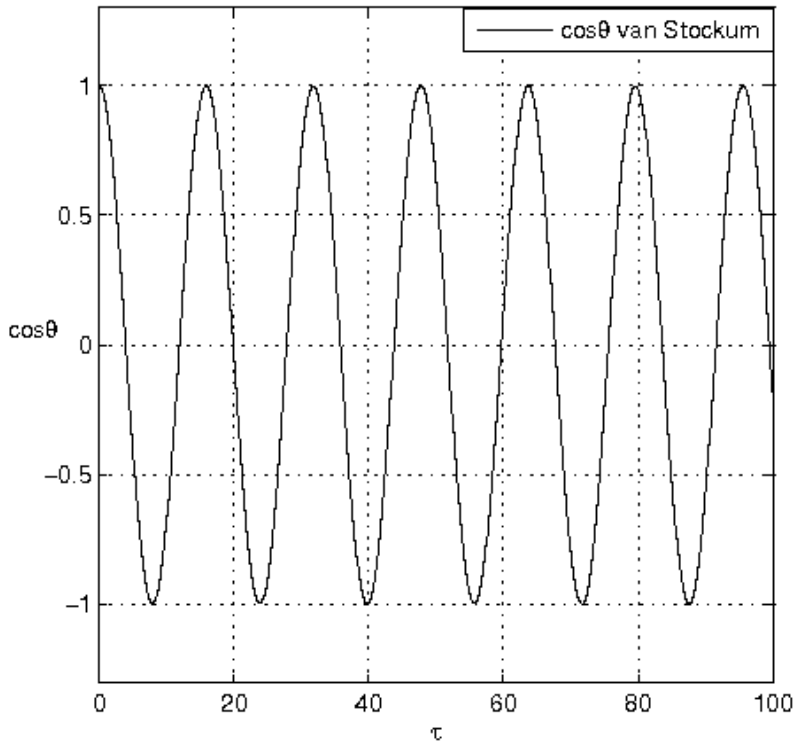

Figure 6.8: The precession of gyroscopes along the forward time oriented timelike orbit of proper circumference $(2\pi)6.5$ with $r = 647.512$ and $p_t = 20.1955$. Note that the frame dragging causes a much greater precession opposite the direction of the rotation of the matter source (the plot has been "squished" and dragged to the left) than the Kerr case.

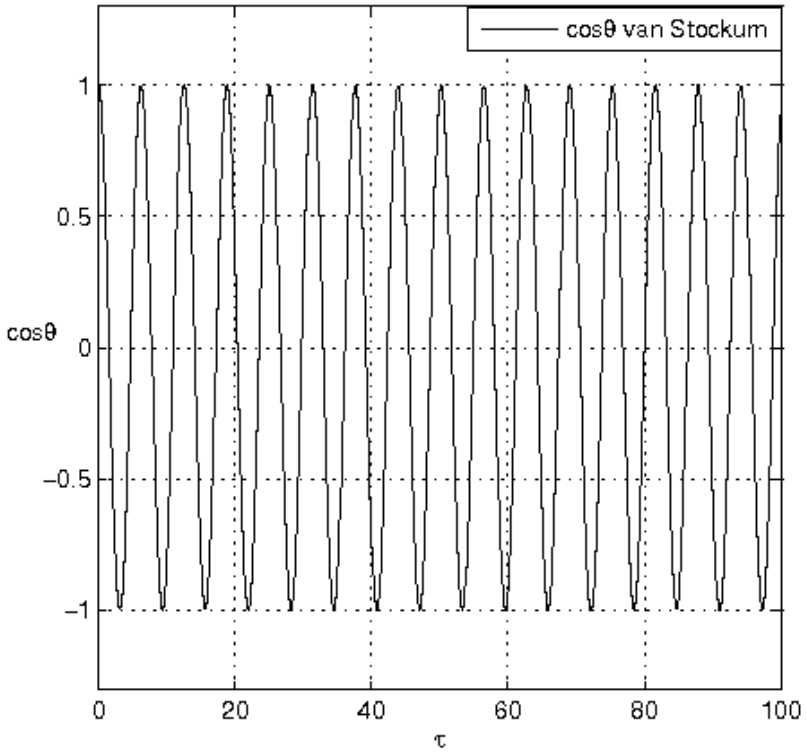

Figure 6.9: Cosine of the angle between initial radial pointing gyroscope with radial component of the spin vector ($s^r(\tau)$ along a CTC in van Stockum metric (xyz projection of is shown in Fig 6.3) for $r = 4.82713$. Note an even greater amount of dragging than in Fig 6.8.

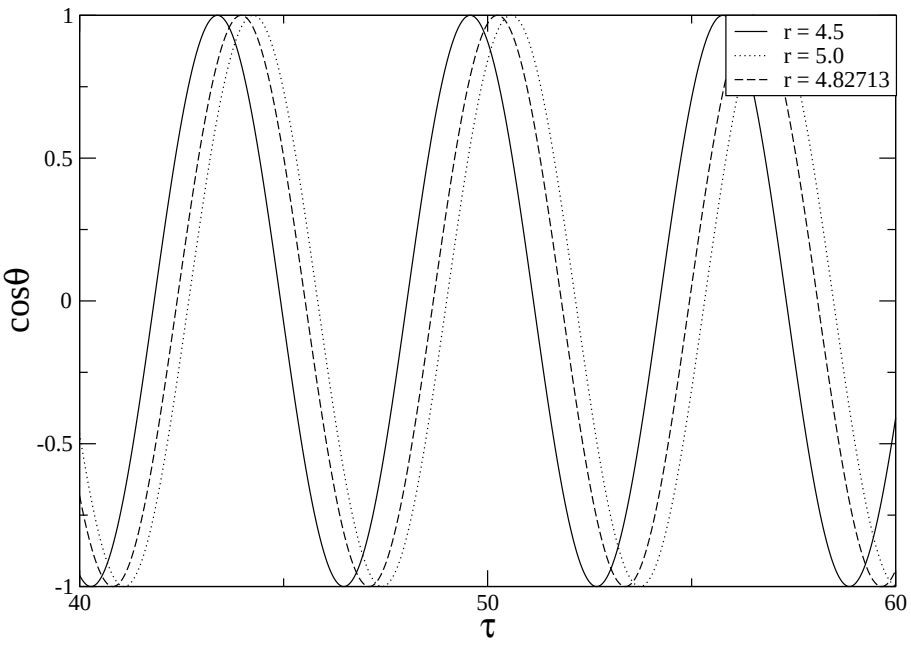

Figure 6.10: A comparison of gyroscope precession for radial distances around the first of the CTC radii.

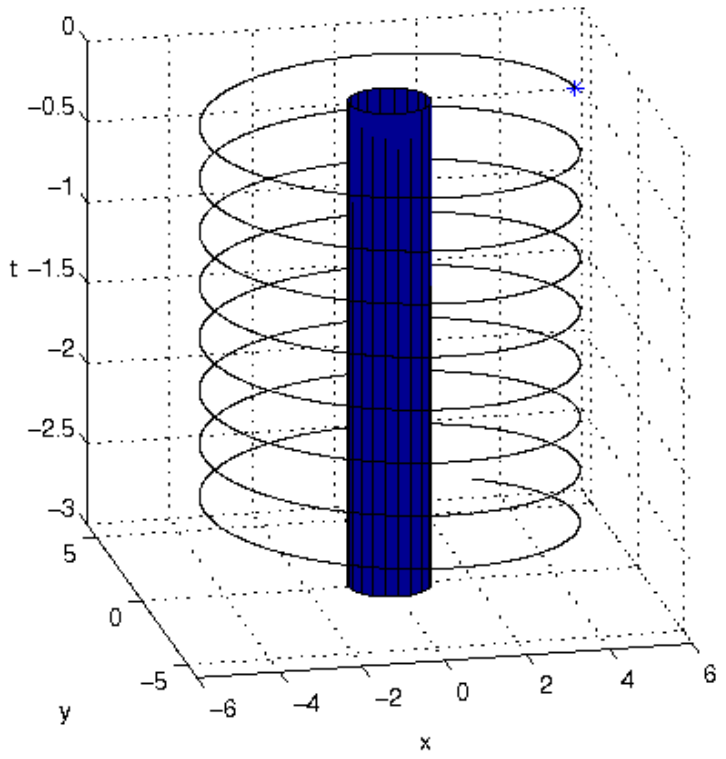

Figure 6.11: The radial geodesic at $r = 4.5$ in Fig 6.10 is a backward in time oriented circular timelike geodesic as also found by Steadman in [15]. The other radius considered in Fig 6.10, $r = 5.0$,is forward in time oriented, as expected.

Chapter 7

Conclusions

In the work of [16], it was hypothesized that CTC's lead observers to counter-rotate against the spacetime rotation and so there must be a secondary mechanism that creates CTC's. In this study, such counter rotation was not found for CTC's or causality violating geodesics in the van Stockum metric, and comparison of the inertial frame dragging of different orbits, such as in in Fig 6.10, appears to support the classical idea that it is greater amounts of inertial frame dragging that cause light cones to tip over, become closed and then become backward in time oriented. In the [16] paper the Kerr-Newman metric was considered so it may be that for the van Stockum metric, with the parameters considered here, does not have such a counter-rotational effect which would expand the mystery of this suggested secondary mechanism for the generation of CTC's as suggested by [16]. However, null lines were not calculated and [16] also claims that the light cones along a CTC also open, rather than become more narrow, so this would be a topic for future work.

A study of the precession of gyroscopes did not suggest any unknown influence as to the source of CTC, and endorses the idea that it is solely due to inertial frame dragging.

7.1 Future Work

The primary avenue for future work would be to attempt to explain the discrepancy between this study and [16] as to the orientation of CTC orbits, and if it is found that observers must counter-rotate in what ways can the probing of gyroscope orbits reveal the source of this remarkable, counter-intuitive behavior? Simulations of the light cone structure of the van Stockum spacetime is also needed to better verify the work of [16] and to gain further insight into the actual causal structure. Finally, analysis and an algorithm to find non-circular orbits that close could help provide a broader interpretation as to the generation of CTC's, as only circular geodesic orbits were considered here.

Appendices

.1 Connection Coefficients for equatorial orbits

Here the connection coefficients are provided for equatorial orbits, $\theta = \pi/2$ for Kerr and $z = 0$ for van Stockum.

.1.1 Kerr Connection

$$\begin{aligned}
\Gamma^0_{01} &= \frac{M(a^2+r^2)}{r^2\Delta} & \Gamma^0_{13} &= \frac{-aM(a^2+3r^2)}{r^2\Delta} \\
\Gamma^1_{00} &= \frac{M\Delta}{r^4} & \Gamma^1_{03} &= -\frac{aM\Delta}{r^4} \\
\Gamma^1_{11} &= \frac{1}{r} + \frac{M-r}{\Delta} & \Gamma^1_{22} &= 2M - \frac{a^2+r^2}{r} \\
\Gamma^1_{33} &= \frac{(a^2M - r^3)\Delta}{r^4} & & \\
\Gamma^2_{12} &= \frac{1}{r} & & \\
\Gamma^3_{01} &= \frac{aM}{r^2\Delta} & \Gamma^3_{13} &= \frac{-a^2M + r^2(-2M+r)}{r^2(a^2 + r(-2M+r))}
\end{aligned} \tag{1}$$

.1.2 van Stockum Connection

For simplification we define:

$$\rho = (\omega a)^2, \qquad \epsilon = \sqrt{4\rho^2 - 1}. \tag{2}$$

And so the connection coefficients are:

$$\begin{aligned}
\Gamma^0_{01} &= \frac{1+\epsilon^2}{4r} & \Gamma^0_{12} &= -\frac{a(1+\epsilon^2)^{3/2}}{8r} \\
\Gamma^2_{01} &= \frac{\sqrt{1+\epsilon^2}}{2ar} & \Gamma^2_{12} &= -\frac{-3+\epsilon^2}{4r} \\
\Gamma^3_{13} &= -\frac{\rho}{r} & & \\
\Gamma^1_{00} &= -\frac{e^{\rho}(r/a)^{2\rho}(1+\epsilon^2)\sin(\gamma)}{2a\epsilon} & &
\end{aligned}$$

$$
\begin{aligned}
\Gamma^1_{02} &= -\frac{e^{\rho}(r/a)^{2\rho}}{2\sin(2\beta)}\left(\epsilon\cos(a\beta+\gamma)+\sin(a\beta+\gamma)\right) \\
\Gamma^1_{22} &= -\frac{e^{\rho}(r/a)^{2\rho}a(1+\epsilon^2)^{3/2}}{8\epsilon}\left(\epsilon\cos(3\beta+\gamma)+\sin(3\beta+\gamma)\right) \\
\Gamma^1_{11} &= -\frac{\rho}{r} \qquad\qquad \Gamma^1_{33} = \frac{\rho}{r}
\end{aligned} \tag{3}
$$

.2 C++ Code

Provided here is the C++ code, written from scratch, for the integration of the geodesic and gyroscope equations for the van Stockum metric. The Runge-Kutta step uses convenient syntax found in [7].

```
 #include <iostream>
using namespace std;
#include <string>
#include <fstream>
#include <cmath>
#include <cstdlib>

const int END_STEP = 800000;
const double a =1.0; // radious of van Stockum cylinder
const double OMEGA = 0.9;
const double RHO = OMEGA*OMEGA*a*a;
const double EPS = sqrt(4*RHO - 1);
const double BETA = atan( EPS );
const int dim = 4; //Dimension of spacetime (usually 4)
const double PI=2.0*asin(1.0);
const double t0 = 0.0, r0 =647.512, Phi0=0, z0 = 0;
// 4.82713, 4.5 cool stuff
const double tDot0 = 0.0, rDot0 = 0.0, PhiDot0 = 0.0, zDot0=0.0; //Lets first try
//const double taustep = 0.01;

//define the vanStockum functions------------------
double H(double [dim]);
double L(double [dim]);
double M(double [dim]);
```

```
double F(double [dim]);
double gamma(double [dim]);
double K(double [dim]);
//---------------------------------------

void f(double [3*dim], double [3*dim]);
void nrk4(double [3*dim], double,
  void (*derivsRK)(double [3*dim], double [3*dim])
  );

int main() {
  double xU[dim], uU[dim], sU[dim], s0U[dim],
state[3*dim], derivs[3*dim], gDD[dim][dim];
  double tau, tplot , xplot , yplot, zplot;
  double metricSum, orthSum, magSum, magSumRoot, sdote;
  double b , c;
  int i; //stepping variable
  int s; //stepping state variable
  int mu, nu , gam; // contra and covarient indexes
  int simStop;

ofstream outfilet("vanStockumGeos.data",ios::out);


//-----------------------------------
/* initialize */
//-----------------------------------

//Initial Positions
  xU[0] = t0;
  xU[1] = r0;
  xU[2] = Phi0;
  xU[3] = z0;

//STEADMAN PAPER
  double pt = -0.515314;
  pt = 20.1955;

  uU[0] = (a*sin(2*BETA + K(xU)))*pt / (2*xU[1]*cos(BETA)*sin(BETA - K(xU)));
```

```
  uU[1] = 0;
  uU[2] = -(sin(K(xU))*pt)/(xU[1]*sin(BETA - K(xU)));
  uU[3] =  0;

 //Initialize metric matrix
for (mu = 0; mu <= 3 ; mu++){
      for(nu =0 ; nu <= 3 ; nu++){
gDD[mu][nu] = 0;
      }
    }

// vanStockum metric functions
 gDD[0][0] = - F(xU);
 gDD[0][2] = M(xU);
 gDD[2][0] = gDD[0][2];
 gDD[1][1] = H(xU);
 gDD[2][2] = L(xU);
 gDD[3][3] = H(xU);

 //The metric sum check
 metricSum = 0;

for (mu = 0; mu <= 3 ; mu++){
      for(nu =0 ; nu <= 3 ; nu++){
metricSum = metricSum + gDD[mu][nu]*uU[mu]*uU[nu];
      }
    }

  cout << metricSum << endl;

  //Initial spins
  sU[0] = 0;
  sU[1] = 1 / sqrt(H(xU));
  sU[2] = 0;
  sU[3] = 0;

// Collect initial spins into initial spin matrix for later

  for(s = 0; s < dim ; s++){
```

```
    s0U[s] = sU[s];
  }


//-----------------------------------------------------
/* main loop of integration steps */
//-----------------------------------------------------
  double taustep = 0.01;

  for (i=1; i <= END_STEP ; i++) {
    tau = i*taustep;

    // Initialize derivative array
        for( s = 0 ; s < 3*dim ; s++){
        derivs[s] = 0;
      }

// Puts all vector components into one state vector to pass to integrator
  state[0] = xU[0];
  state[1] = xU[1];
  state[2] = xU[2];
  state[3] = xU[3];
  state[4] = uU[0];
  state[5] = uU[1];
  state[6] = uU[2];
  state[7] = uU[3];
  state[8] = sU[0];
  state[9] = sU[1];
  state[10] = sU[2];
  state[11] = sU[3];

  nrk4(state, taustep, f);

   //put back into 4-vector notation for convenience
  xU[0] = state[0];
  xU[1] = state[1];
  xU[2] = state[2];
  xU[3] = state[3];
  uU[0] = state[4];
```

```
  uU[1] = state[5];
  uU[2] = state[6];
  uU[3] = state[7];
  sU[0] = state[8];
  sU[1] = state[9];
  sU[2] = state[10];
  sU[3] = state[11];

  //-------------------------------------------------
  //Checks on the Integration by calculating constraints
  //-------------------------------------------------

  //Initialize metric matrix
for (mu = 0; mu <= 3 ; mu++){
      for(nu =0 ; nu <= 3 ; nu++){
gDD[mu][nu] = 0;
      }
    }

// vanStockum metric functions
 gDD[0][0] = - F(xU);
 gDD[0][2] = M(xU);
 gDD[2][0] = gDD[0][2];
 gDD[1][1] = H(xU);
 gDD[2][2] = L(xU);
 gDD[3][3] = H(xU);

 //The metric sum check
 metricSum = 0;

for (mu = 0; mu <= 3 ; mu++){
      for(nu =0 ; nu <= 3 ; nu++){
metricSum = metricSum + gDD[mu][nu]*uU[mu]*uU[nu];
      }
    }

//Spin metric sum checks
 orthSum = 0;
```

```
for (mu = 0; mu <= 3 ; mu++){
      for(nu =0 ; nu <= 3 ; nu++){
orthSum = orthSum + gDD[mu][nu]*uU[mu]*sU[nu];
      }
    }

//Spin Magnitude check (here s_* = 1)
 magSum = 0;

for (mu = 0; mu <= 3 ; mu++){
      for(nu =0 ; nu <= 3 ; nu++){
magSum = magSum + gDD[mu][nu]*sU[mu]*sU[nu];
      }
    }

 magSumRoot = sqrt(magSum);

 //Calculate the dot product with initial spin array

 sdote = 0;

 for (mu = 0; mu <= 3 ; mu++){
      for(nu =0 ; nu <= 3 ; nu++){
sdote = sdote + gDD[mu][nu]*sU[mu]*s0U[nu];
      }
    }

//------------------------------------------------------------

   // Cartesian for Plotting
   tplot = xU[0];
   xplot = xU[1] * cos(xU[2]);
   yplot = xU[1] * sin(xU[2]);
   zplot = xU[3];

   //  outfilet << tplot << " " << xplot << " " << yplot <<" " << zplot << " " <<
   // outfilet << xU[0] << " " << xU[1] << " " << xU[2] << " " << xU[3] << " " <<
   // outfilet <<  metricSum << " " << orthSum << " " << magSumRoot << endl;
   //outfilet << tau << " " << sU[1] << " " << sU[3] << endl;
```

```
    outfilet << tau << " " << sdote << endl;

   // if(metricSum > -.999995 or  metricSum < -1.000005){
   //     cout << tplot << " " << tau << endl;
   //     break;
   //   }

      if(i == END_STEP){
      cout << tplot << " " << tau << endl;
       }

  }

  return 0;
}

/*---------------------------------------
/ LHS of differential equation for integration
/---------------------------------------
*/

void f(double state[3*dim], double derivs[3*dim]){

 double DuU0, DuU1, DuU2 , DuU3;
  double DsU0, DsU1, DsU2 , DsU3;
  double GammaUDD[dim][dim][dim];
 int mu, nu , gam;

double xU[dim], uU[dim], sU[dim];

  xU[0] = state[0];
  xU[1] = state[1];
  xU[2] = state[2];
  xU[3] = state[3];
  uU[0] = state[4];
  uU[1] = state[5];
  uU[2] = state[6];
  uU[3] = state[7];
```

```
  sU[0] = state[8];
  sU[1] = state[9];
  sU[2] = state[10];
  sU[3] = state[11];

// Initialize Gammas to 0 at beggining of each loop

for (mu = 0; mu <= 3 ; mu++){
      for(nu =0 ; nu <= 3 ; nu++){
for (gam = 0 ; gam <= 3 ; gam++){
  GammaUDD[mu][nu][gam]=0;
}
      }
    }

  //Put in non-trivial Gammas, using symmetry of the connection
 GammaUDD[0][0][1] = (1 + EPS*EPS)/(4*xU[1]);
 GammaUDD[0][1][0] = GammaUDD[0][0][1];
 GammaUDD[0][1][2] = - a * pow(1 + EPS*EPS, 1.5) / (8*xU[1]);
 GammaUDD[0][2][1] = GammaUDD[0][1][2];

GammaUDD[1][0][0] = - exp(RHO)*pow(xU[1]/a,2*RHO)*(1+
EPS*EPS)*sin(EPS*log(xU[1]/a))/(2*a*EPS);
GammaUDD[1][0][2] =
-0.5*exp(RHO)*pow(xU[1]/a,2*RHO)*(EPS*cos(atan(EPS)+
EPS*log(xU[1]/a))+ sin(atan(EPS)+EPS*log(xU[1]/a)))/(sin(2*atan(EPS)));
GammaUDD[1][2][0] = GammaUDD[1][0][2];
GammaUDD[1][1][1] = - RHO / xU[1];
GammaUDD[1][2][2] = - a *exp(RHO)*pow(xU[1]/a,2*RHO)*pow(1+
EPS*EPS, 1.5)*(1/(8*EPS))*(EPS*cos(3*atan(EPS)+EPS*log(xU[1]/a))+
sin(3*atan(EPS)+
EPS*log(xU[1]/a)));
GammaUDD[1][3][3] = RHO/xU[1];

 GammaUDD[2][0][1] = sqrt(1 + EPS*EPS)/(2*a*xU[1]);
 GammaUDD[2][1][0] = GammaUDD[2][0][1];
 GammaUDD[2][1][2] = - (-3 + EPS*EPS) / (4*xU[1]);
 GammaUDD[2][2][1] = GammaUDD[2][1][2];
```

```
 GammaUDD[3][1][3] = - RHO / xU[1];
 GammaUDD[3][3][1] = GammaUDD[3][1][3];

 //Take derivatives of four velocity

  DuU0 = 0;
  DuU1 = 0;
  DuU2 = 0;
  DuU3 = 0;

    for(nu= 0 ; nu <= 3 ; nu++){
      for(gam= 0 ; gam <= 3 ; gam++){
DuU0 = DuU0 - GammaUDD[0][nu][gam]*uU[nu]*uU[gam];
DuU1 = DuU1 - GammaUDD[1][nu][gam]*uU[nu]*uU[gam];
DuU2 = DuU2 - GammaUDD[2][nu][gam]*uU[nu]*uU[gam];
DuU3 = DuU3 - GammaUDD[3][nu][gam]*uU[nu]*uU[gam];
      }
    }

    // Take derivatives of spins
  DsU0 = 0;
  DsU1 = 0;
  DsU2 = 0;
  DsU3 = 0;

for(nu= 0 ; nu <= 3 ; nu++){
      for(gam= 0 ; gam <= 3 ; gam++){
DsU0 = DsU0 - GammaUDD[0][nu][gam]*sU[nu]*uU[gam];
DsU1 = DsU1 - GammaUDD[1][nu][gam]*sU[nu]*uU[gam];
DsU2 = DsU2 - GammaUDD[2][nu][gam]*sU[nu]*uU[gam];
DsU3 = DsU3 - GammaUDD[3][nu][gam]*sU[nu]*uU[gam];
      }
    }

//Assembles the derivative array
  derivs[0] =  uU[0];
  derivs[1] =  uU[1];
  derivs[2] =  uU[2];
  derivs[3] =  uU[3];
```

```
  derivs[4] =  DuU0;
  derivs[5] =  DuU1;
  derivs[6] =  DuU2;
  derivs[7] =  DuU3;
  derivs[8] =  DsU0;
  derivs[9] =  DsU1;
  derivs[10] =  DsU2;
  derivs[11] =  DsU3;

}

//---------------------------
// vanStockum functions
//---------------------------
double gamma(double xU[dim]){
  double valueGamma;
  valueGamma = EPS*log(xU[1]/a);
  return valueGamma;
}

double H(double xU[dim]){
  double valueH;
  valueH = exp(-RHO)*pow( xU[1]/a , -2 * RHO);
  return valueH;
}

double L(double xU[dim]){
  double valueL;
  valueL = a*xU[1]*sin(3*BETA + gamma(xU))/(2*sin(2*BETA)*cos(BETA));
  return valueL;
}

double M(double xU[dim]){
  double valueM;
  valueM = xU[1]*sin(BETA + gamma(xU))/sin(2*BETA);
  return valueM;
}

double F(double xU[dim]){
```

```
  double valueF;
  valueF = xU[1]*sin(BETA - gamma(xU))/(a*sin(BETA));
  return valueF;
}

double K(double xU[dim]){
  double valueK;
  valueK = 0.5*log(xU[1]/a)*EPS;
  return valueK;
}


/*---------------------------------------
/ Fourth Order Runge Kutta
/--------------------------------------
*/

void nrk4(double state[3*dim], double taustep,// state, taustep
  void (*derivsRK)(double state[3*dim], double derivs[3*dim]) //state tau derivs
  ){

  double *F1, *F2, *F3, *F4, *tempState;
  int i;
  F1 = new double [3*dim];
  F2 = new double [3*dim];
  F3 = new double [3*dim];
  F4 = new double [3*dim];
  tempState = new double [3*dim];

  //Calculate F1
  (*derivsRK)(state, F1);

  //Calulate F2
  //double half_taustep = 0.5*taustep;
  for(i = 0; i < 3*dim ; i++){
    tempState[i] = state[i] + 0.5*taustep*F1[i];
  }
(*derivsRK)(tempState, F2);
```

```
//Calculate F3
 for(i = 0; i < 3*dim ; i++){
    tempState[i] = state[i] + 0.5*taustep*F2[i];
  }
(*derivsRK)(tempState, F3);

//Calculate F4
 for(i = 0; i < 3*dim ; i++){
   tempState[i] = state[i] + taustep*F3[i];
  }
(*derivsRK)(tempState, F4);


  for(i = 0; i < 3*dim; i++){
    state[i] = state[i] + (taustep/6.0)*(F1[i] + F4[i] + 2.0*(F3[i] + F2[i]));
  }

  delete [] F1, F2, F3, F4, tempState;
}
```

References

[1] Hartle, B. James. *Gravity: An Introduction to Einstein's General Relativity*. Pearson Education, Inc. San Francisco, CA 2003

[2] Tipler, Frank J. *Rotating cylinders and the possibility of global causality violation*. Physical Review. Vol 9 Num 8. April 1974

[3] W.J. van Stockum. *The Gravitational Field of a Distribution of Particles Rotating about an Axis of Symmetry*. Proc. Roy. Soc. Edinburgh **57**: 135 (1936)

[4] Slobodov, Sergei. *Unwrapping Closed Timelike Curves*. Found. Phys. **38**: 1082-1109 (2008)

[5] Collas, Peter and Klein, David. *Causality Violating Geodesics in Bonnor's Rotating Dust Metric*. Gen. Rel. Gravitation. **36** No.11 Nov. 2004

[6] Butcher, J. C. *Numerical Methods for Ordinary Differential Equations*. John Wiley & Sons, Ltd. England 2008

[7] Garcia, Alejandro L. *Numerical Methods for Physics*. Prentice-Hall, Inc. NJ 2000

[8] F. I. Cooperstock and S. Tieu. Found. Phys. **35** 1497 (2005).

[9] Carter, Brandon. *Global Structure of the Kerr Family of Gravitational Fields*. Physical Review. **174** Num 5 (1968)

[10] Bonnor B. W. *An exact, asymptotically flat, vacuum solution of Einstein's equations with closed timelike curves*. Class. Quantum Grav. **19** (2002)

[11] Hobson, M. P., Efstathiou G. and Lasenby A.N. *General Relativity: An Introduction for Physicists*. Cambridge University Press. Cambridge 2006

[12] Misner, Charles W., Thorne, Kip S. and Wheeler, John A. *Gravitation*. W.H. Freeman and Company. New York. 1973

[13] Chandrasekhar S. *The Mathematical Theory of Black Holes*. Oxford University Press. New York. 1983

[14] Price, Richard H. *General Relativity Primer*. Am. J. Phys. **40** 4, (1982)

[15] Steadman R. B. *Causality Violation on van Stockum Geodesics*. Gen. Rel. Grav **35** 9 (2003)

[16] Andréka, Hajnal. Németi, István. Wűthrich, Christian. *A twist in the gepmetry of rotating black holes: seeking the cause of acausality*. Gen. Rel. Grav. **40** 1809-1823 (2008)

[17] Lobo, F. Crawford, P. *Time, Closed Timelike Curves and Causality*. NATO Sci. Ser. **11** 95 (2003)